https://doi.org/10.5194/egusphere-2026-5476
Preprint. Discussion started: 11 September 2026

What controls tropospheric carbon monoxide in the remote Southern Hemisphere?

Clara M. Nussbaumer[1], Colette L. Heald[1], Teresa Campos[2], Eric A. Kort[3,4], Paul B. Krummel[5], Ray L. Langenfelds[5], Monica Madronich[6,7], Kathryn McKain[7], Gabrielle Pétron[6,7], Ann Stavert[5], and Steven C. Wofsy[8]

[1]Institute for Atmospheric and Climate Science (IAC), ETH Zürich, Zürich, Switzerland
[2]Atmospheric Chemistry Observations and Modeling (ACOM) Laboratory, NSF National Center for Atmospheric Research (NCAR), Boulder, CO, USA
[3]Climate and Space Sciences and Engineering, University of Michigan, Ann Arbor, MI, USA
[4]Department of Atmospheric Chemistry, Max Planck Institute for Chemistry, Mainz, Germany
[5]CSIRO Environment, Aspendale, Victoria, Australia
[6]Cooperative Institute for Research in Environmental Sciences, University of Colorado Boulder, Boulder, Colorado, USA
[7]NOAA Global Monitoring Laboratory, Boulder, Colorado, USA
[8]Harvard John A. Paulson School of Engineering and Applied Sciences, Harvard University, Cambridge, MA, USA

Correspondence: Clara M. Nussbaumer (clara.nussbaumer@env.ethz.ch) and Colette L. Heald (colette.heald@env.ethz.ch)

Abstract. The remote extratropical Southern Hemisphere (SH) has the cleanest atmosphere on Earth, but is subject to rapid changes regarding the emissions landscape and a warming climate, which strongly impact local atmospheric composition. Carbon monoxide (CO) is a product of methane (CH_4) oxidation and a modulator of the tropospheric oxidizing capacity. In this study we investigate if the rapid increase in tropospheric CH_4 levels of ∼7 % between 2008 and 2022 has driven a positive response in CO in the remote SH, based on multi-platform observations and a global chemistry transport model. We find inconsistencies in observations from aircraft, surface and satellite. CSIRO surface flask observations, AGAGE in-situ measurements (2008–2022) and airborne observations from the HIPPO (2009–2011) and ATom (2016–2018) campaigns show CO increases of 5–10 %. CO columns inferred from IASI (2014–2023) show more moderate increases of 3–4 % (statistically insignificant). NOAA surface flask observations and CO columns from MOPITT (2008–2022) do not show changes over time. GEOS-Chem simulations are consistent with the observed positive trend, exhibiting a significant CO increase of ∼7 % throughout the southern extratropical troposphere (2008–2022). These CO increases are partly driven by enhanced production from rising CH_4 (∼50 %) and further affected by increases in biogenic non-methane volatile organic compounds (NMVOC) (∼45 %) and the direct effects of rising temperatures (∼5 %). We further explore how simulated CO levels in the remote SH could be impacted by future enhancements in primary and precursor emissions, changes in the oxidizing capacity, and temperature.

1 Introduction

The Southern Hemisphere (SH) has historically been less impacted by anthropogenic pollution than the Northern Hemisphere (NH) and is often viewed as a proxy for the preindustrial atmosphere (Paton-Walsh et al., 2022). However, even remote SH

https://doi.org/10.5194/egusphere-2026-5476
Preprint. Discussion started: 11 September 2026

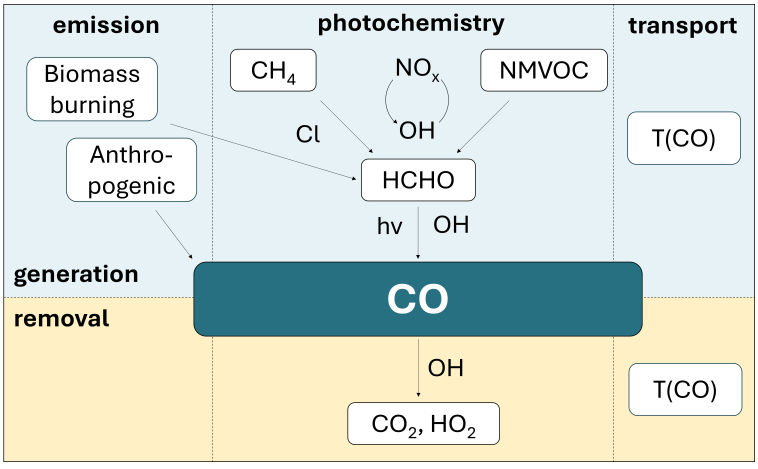

Figure 1. Overview of processes which impact carbon monoxide concentrations in the troposphere.

regions are increasingly affected by anthropogenic influences related to ongoing industrialization, a growing population in the Global South, and climate change, all of which are expected to accelerate in the future. The United Nations Department of Economic and Social Affairs, Population Division (2022) predicts a population increase of around 15% in Latin America and the Caribbean and of more than 80% in Sub-Saharan Africa between 2022 and 2050. van der Zwaan et al. (2018) estimates a concurrent increase in African greenhouse gas emissions from 8% to 18% of global emissions between 2010 and 2050 (when limiting global warming to 2 °C). Vohra et al. (2022) predicts that rapid increases in the number of tropical megacities (from 12 to 46 between 2020 and 2100), mostly located in Africa, India, Southeast Asia and South America, will coincide with continuous increases in pollutant and greenhouse gas emissions, which will likely affect the chemical composition of the atmosphere in the Southern Hemisphere. At the same time, the SH has limited in-situ atmospheric observations, largely due to the preponderance of NH-based researchers and the historic focus on the effects of anthropogenic pollution in the NH (Paton-Walsh et al., 2022). An additional challenge is posed by the large surface share of oceans, which limits the possibilities for land-based observations. Uncertain emission projections of CO and related trace gases under different SSP (Shared Socioeconomic Pathways) scenarios (Riahi et al., 2017) combined with the SH's unique characteristics, such as enhanced solar intensity, and the scarcity of in-situ observations compared to the Northern Hemisphere create an urgent need to focus efforts on advancing our understanding of the processes controlling atmospheric composition in the Southern Hemisphere.

Tropospheric carbon monoxide (CO) plays an important role in regulating the oxidizing capacity of the troposphere via reaction with OH radicals, which in turn impacts the lifetime of greenhouse gases, such as methane (CH_4), and other air pollutants, such as ozone (O_3) (Levy, 1971; Logan et al., 1981). Additionally, CO is a precursor to tropospheric ozone formation. It is often used as an indicator for long range transport of air pollution (Jaffe et al., 1997; Pope et al., 2021; Heald et al., 2003).

Carbon monoxide is affected by various processes in the troposphere, including emissions, photochemistry, and transport (Zheng et al., 2019). We present an overview of these processes in Figure 1. Anthropogenic emissions are dominated by combustion processes, including on-road vehicles, industrial activities, residential burning, shipping, and aviation (Holloway

https://doi.org/10.5194/egusphere-2026-5476
Preprint. Discussion started: 11 September 2026

et al., 2000; Seinfeld and Pandis, 2016). Furthermore, biomass burning is a large direct source of carbon monoxide (Crutzen et al., 1979; Griffin et al., 2024). A small share of global CO is emitted from ocean surfaces via the oxidation of dissolved organic matter (DOM) (Swinnerton et al., 1970; Conte et al., 2019). Secondary tropospheric CO is formed via the oxidation of CH_4 and the oxidation of non-methane volatile organic compounds (NMVOC) with formaldehyde (HCHO) as an important intermediate (Levy II, 1973; Poisson et al., 2000).

$$CH_4 + OH \rightarrow CH_3 + H_2O \quad \text{(R1)}$$

$$CH_3 + O_2 \rightarrow CH_3O_2 \quad \text{(R2)}$$

$$CH_3O_2 + NO \rightarrow CH_3O + NO_2 \quad \text{(R3a)}$$

$$CH_3O_2 + HO_2 \rightarrow CH_3OOH + O_2 \quad \text{(R3b)}$$

$$CH_3O + O_2 \rightarrow HCHO + HO_2 \quad \text{(R4a)}$$

$$CH_3OOH \xrightarrow{h\nu/OH} HCHO \quad \text{(R4b)}$$

Reactions (R1)–(R4b) present the formation of HCHO from CH_4. In the first step, an OH radical reacts with CH_4 to form CH_3. While OH is the dominant oxidant of CH_4 in the atmosphere, reaction (R1) can also proceed with a different oxidant such as chlorine (Cl) radicals (Platt et al., 2004). CH_3 rapidly forms CH_3O_2 in the presence of O_2. The peroxy radical is then either reduced to an alkoxy radical CH_3O via reaction with NO that forms NO_2 (R3a) or reacts with HO_2 to form methyl hydroperoxide (CH_3OOH) (R3b). CH_3O reacts with O_2 to HO_2 and HCHO (R4a) and CH_3OOH forms HCHO through photolysis or oxidation via OH (R4b). HCHO can subsequently form CO via oxidation or photolysis as shown in Reactions (R5)–(R7) (Levy II, 1973). Besides photochemical loss, HCHO can also be removed via both dry and wet deposition (Thompson, 1980).

$$HCHO + OH + O_2 \rightarrow CO + HO_2 + H_2O \quad \text{(R5)}$$

$$HCHO \xrightarrow{h\nu} CO + H_2 \quad \text{(R6)}$$

https://doi.org/10.5194/egusphere-2026-5476
Preprint. Discussion started: 11 September 2026

$$HCHO + 2O_2 \xrightarrow{h\nu} CO + 2HO_2 \quad \text{(R7)}$$

The formation of CO from NMVOCs proceeds in a similar way via the analogous peroxy (RO_2) and alkoxy radicals (RO), whereby the generation of HCHO from RO can involve multiple oxidation steps, depending on the nature of the organic rest (R). Additionally, the peroxy radical can form HCHO through reaction with HO_2 (via ROOH) or internal H-shifts (Carlier et al., 1986; Poisson et al., 2000). The multi-generational oxidation of NMVOCs and the resulting products ultimately produce HCHO (Seinfeld and Pandis, 2016). Beyond VOC oxidation, HCHO can also be emitted directly from anthropogenic combustion processes, biomass burning and vegetation. Secondary HCHO formation prevails as a contributor to the global HCHO budget, but direct emissions can dominate locally (e.g. Lee et al. (1998); Fortems-Cheiney et al. (2012)).

The loss of CO occurs predominantly through the oxidation with OH radicals as shown in Reaction (R8), which is an important mechanism for controlling the oxidizing capacity of the atmosphere. Dry and wet deposition are negligible as CO loss pathways.

$$CO + OH \rightarrow CO_2 + H \quad \text{(R8)}$$

The lifetime of CO is dependent on latitude and season, but is on the order of several weeks to months (Weinstock, 1969; Khalil and Rasmussen, 1990; Holloway et al., 2000). Therefore, it can be transported within one hemisphere, while inter-hemispheric mixing is negligible (Bowman, 2006; Gloudemans et al., 2006).

Ice core and firn air measurements constrain the evolution of tropospheric carbon monoxide over the past several centuries. Between preindustrial times and the 1980s, CO levels have significantly increased both in the Northern and Southern Hemisphere by around 50–60 % mostly related to rising emission from anthropogenic combustion processes (Faïn et al., 2022, 2023; Strawson et al., 2024). These positive CO trends reversed in the late 1980s / early 1990s and CO levels have subsequently decreased globally. Early records of declining CO go back to the implementation of long-term surface networks (Novelli et al., 1994, 1998; Patel et al., 2024; World Meteorological Organization, 2025). These include, for example, the NOAA GML cooperative air sampling network and the CSIRO Global Atmospheric Sampling LABoratory (GASLAB) (CSIRO, 2021; NOAA, 2025), which provide continuous records since the 1980s. Findings from the surface networks are supported by satellite retrievals from the MOPITT (Measurement of Pollution in the Troposphere) instrument from the early 2000s onward, often in combination with global model simulations (Worden et al., 2013; Yoon and Pozzer, 2014; Yin et al., 2015; Hedelius et al., 2021). The magnitude of this CO decline is highly regional with up to 25 % in the Northern Extratropics and around 10 % as a global average between 1995 and 2020 (World Meteorological Organization, 2025). It is driven by the introduction of catalytic converters on vehicles as well as cleaner burning fuels, which lead to strong reductions in CO emissions, particularly from developed countries in the Northern Hemisphere (Jiang et al., 2017; IPCC, 2021; Soulie et al., 2024). More recently, several studies suggest an attenuation of the CO decline rate around the globe (Jiang et al., 2018; Buchholz et al., 2021; Okpalaonwuka et al., 2024; Patel et al., 2024). Potential explanations include a deceleration of anthropogenic CO emission reductions

https://doi.org/10.5194/egusphere-2026-5476
Preprint. Discussion started: 11 September 2026

and enhanced fire related emissions, which counteract the fossil fuel CO declines (Jiang et al., 2018; Zheng et al., 2021; Soulie et al., 2024).

In this study, we investigate processes that affect carbon monoxide in the Southern Hemisphere. We focus on CO changes in the remote SH, which is primarily represented by the southern extratropics at latitudes south of 30°S. In contrast to the tropics, where CO is more strongly influenced by large, variable emissions (Tsivlidou et al., 2023), CO levels in the remote SH are driven by both photochemical production and transported primary emissions, enabling the identification of long-term changes in the Southern Hemispheric background. While the important CO precursor CH_4 was mostly constant between 2000 and 2007, concentrations have rapidly increased since 2008 (Rigby et al., 2017; Saunois et al., 2025; Lan et al., 2026). We explore to what degree this large increase in tropospheric CH_4 levels has caused enhancements in remote SH carbon monoxide. We use a suite of surface (NOAA GML and CSIRO flasks and AGAGE in-situ), airborne (ATom and HIPPO) and satellite observations (MOPITT, IASI, and OMI) in combination with a global model (GEOS-Chem) to study recent CO trends in the SH. In addition to the increasing methane, we investigate the current and potential future contributions of changing anthropogenic and biomass burning CO emissions, precursor levels, and temperature.

2 Methods

2.1 Observational data

We use discrete surface air sample (flask) CO measurements of the NOAA Global Monitoring Laboratory (GML) and the Commonwealth Scientific and Industrial Research Organisation (CSIRO), in-situ surface data from the Advanced Global Atmospheric Gases Experiment (AGAGE), as well as in-situ high-frequency CO measurements from the HIPPO (HIAPER Pole-to-Pole Observations) and ATom (Atmospheric Tomography Mission) flight campaigns South of 30°S latitude. Figure 2 shows an overview of the location of these measurements. We further investigate satellite retrievals of CO partial tropospheric columns from the MOPITT and IASI (Infrared Atmospheric Sounding Interferometer) instruments. We investigate the observational trends of CO between 2008 and 2022, or according to availability (Table S1).

2.1.1 Surface measurements

The NOAA GML and the CSIRO provide long-term and calibrated flask measurements of trace gases around the globe (NOAA GML, 2025a; Francey et al., 2003; Langenfelds et al., 2026). For this analysis, we use NOAA CO flask data provided by Pétron et al. (2026) and CSIRO CO flask data, which is available from the World Data Center for Greenhouse Gases (WDCGG) (2025). We use measurements collected at sampling sites which are located at southern extratropical latitudes (LAT $>$ 30°S) and which have a continuous record of carbon monoxide measurements of at least 10 years between 2008 and 2022. These criteria result in a total of 5 CSIRO surface air sampling sites (site IDs: CGO, CYA, MAA, MQA and SPO) and 9 NOAA sites (site IDs: BHD, CGO, CPT, CRZ, DRP, PSA, SPO, SYO and USH). We show their locations in Figure 2 as light blue circles and dark blue squares, respectively. At the sites CGO and SPO, both CSIRO and NOAA flask observations are available. Additionally at

https://doi.org/10.5194/egusphere-2026-5476
Preprint. Discussion started: 11 September 2026

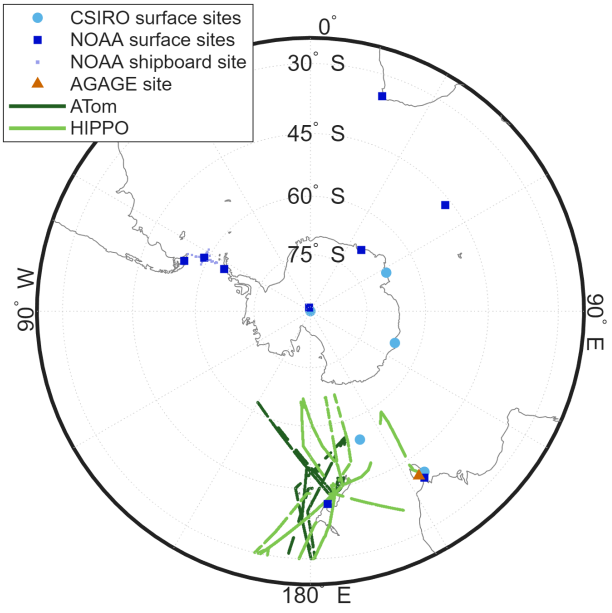

Figure 2. Overview of the observations used in this study. Blue markers show the position of the investigated CSIRO (light blue circles) and NOAA GML (dark blue squares) surface flask sites. Smaller blue squares indicate the measurement location of the shipboard flask. The average of these shipboard coordinates is marked as dark blue square at 59.04°S latitude and 63.33°W longitude. The location of the continuous CO AGAGE measurement is marked as orange triangle. ATom and HIPPO flight tracks are shown in dark and light green, respectively. The airborne data are filtered for the southern extratropics and for the troposphere (0.003 ppb ppm^{-1} < O_3/H_2O < 1 ppb ppm^{-1}).

CGO, continuous CO measurements are available as part of the AGAGE (Advanced Global Atmospheric Gases Experiment) network (Prinn et al., 2018, 2025). The site DRP is located on a ship and its exact measurement location varies. We highlight individual coordinates as light blue squares and the average location as a dark blue square at 59.04°S latitude and 63.33°W longitude. Table S2 of the Supplement provides an overview of additional site information. We only include measurements that are flagged as representative of the background in the analysis. For the multi-year trend analysis we follow the curve fitting method described in NOAA GML (2025b), based on Thoning et al. (1989). We use the default curve fitting parameters and set the data gap limit to 90 days for linear interpolation. Yearly averages are calculated from the deseasonalized time series. The measurement frequency varies among sites (mostly between 1 and 3 weeks), but is mostly consistent at the individual sites over time (Figure S1). We determine the composite mean as the average of the yearly site means (giving each site equal weight). The uncertainty of the averages is represented by the root mean square value of the standard deviations of each site based on the deseasonalized data. We fit a linear regression model to the yearly averages to assess the change over time. The flask measurements from CSIRO and the CGO AGAGE observations are on the CSIRO2020 calibration scale. The NOAA CO measurements are on the WMO CO X2025 calibration scale, which was recently updated from the WMO CO X2014A scale. Details are provided by the NOAA Global Monitoring Laboratory (2026). Therefore, the NOAA and CSIRO data are not directly comparable due to calibration scale differences.

https://doi.org/10.5194/egusphere-2026-5476
Preprint. Discussion started: 11 September 2026

2.1.2 HIAPER Pole-to-Pole Observations 2009–11 (HIPPO)

The HIPPO campaign included five deployments between 2009 and 2011 with the NSF (National Science Foundation) NCAR (National Center for Atmospheric Research) HIAPER (High-performance Instrumented Airborne Platform for Environmental Research) Gulfstream GV aircraft (UCAR/NCAR - Earth Observing Laboratory, 2005; Wofsy et al., 2011). The deployments occurred in different times of the year, including January 2009 (HIPPO-1), October-December 2009 (HIPPO-2), March-April 2010 (HIPPO-3), May-July 2011 (HIPPO-4) and August-September 2011 (HIPPO-5) and covered the Pacific Ocean between the North and the South Pole (UCAR/NCAR - Earth Observing Laboratory, 2011). We filter for tropospheric data using the ratio of O_3 to H_2O ($0.003\,\mathrm{ppb\,ppm^{-1}} < O_3/H_2O < 1\,\mathrm{ppb\,ppm^{-1}}$) as suggested by Bourgeois et al. (2021). We additionally filter for longitudes, where HIPPO and ATom data are geographically overlapping, which are between 150°W and 180°W, as well as between 100°E and 180°E longitude. We exclude measurements over the Australian continent. The HIPPO flight tracks are shown in light green in Figure 2. Carbon monoxide was measured via quantum cascade laser absorption spectroscopy with an accuracy of 3.5 ppbv and a precision of 0.5 ppbv (1 Hz). Instrumental details are provided in Santoni et al. (2014). CO was additionally measured via vacuum UV resonance fluorescence (Aero-Laser AL5002) with an uncertainty of 2 ppbv+3 % (2 s) (Bourgeois et al., 2020). These two CO measurements were combined into a joint dataset (CO.X) based on the best available data, which we use for this analysis. The CO.X data is calibrated to the X2004 scale, which preceded both the current X2025 and previous X2014A scale. Therefore, we additionally use CO observations from the Programmable Flask Package (PFP) calibrated on the WMO X2025 scale (McKain et al., 2026). The O_3 and H_2O mixing ratios used in our filter were measured via UV absorption and through tunable diode laser spectrometry, respectively (Bourgeois et al., 2020).

2.1.3 Atmospheric Tomography Mission 2016–18 (ATom)

ATom was carried out between 2016 and 2018 with the NASA DC-8 research aircraft. Four deployments took place in July-August 2016 (ATom-1), January-February 2017 (ATom-2), September-October 2017 (ATom-3), and April-May 2018 (ATom-4), each of which flew pole to pole over the Pacific and Atlantic ocean basins. More details on the campaign are provided in Thompson et al. (2022). For this study, we include data from all deployments South of 30°S latitude and within the troposphere. In accordance with the HIPPO data processing, we filter for tropospheric data ($0.003\,\mathrm{ppb\,ppm^{-1}} < O_3/H_2O < 1\,\mathrm{ppb\,ppm^{-1}}$) South of 30°S latitude and with HIPPO overlapping longitudes. The resulting flight tracks are shown in dark green in Figure 2. Carbon monoxide was measured via quantum cascade laser absorption spectroscopy (identical instrument as used for HIPPO). CO was additionally measured with a cavity ring-down spectrometer, with an uncertainty of 5 ppbv (1 Hz) (McKain and Sweeney, 2021). We use the CO.X merged product based on the best available data. The ATom CO data are calibrated using the WMO X2014A calibration scale. We further use ATom CO observations from the Programmable Flask Package (PFP) on the WMO X2025 calibration scale to ensure that HIPPO and ATom data can be directly compared (both on X2025 scale) (McKain et al., 2026). We use O_3 measured via chemiluminescence (with nitric oxide) and water vapor measured with a diode laser hygrometer for our stratospheric air data filter (Bourgeois et al., 2020).

https://doi.org/10.5194/egusphere-2026-5476
Preprint. Discussion started: 11 September 2026

2.1.4 MOPITT Satellite Observations

We investigate carbon monoxide retrievals from the MOPITT instrument onboard NASA's Terra satellite. We use measurements from 2001 to 2023. The local overpass time is 10:30 (both AM and PM). MOPITT measures the spectral radiance in the infrared range using gas filter correlation radiometry (George et al., 2015). We use the monthly gridded Level 3 daytime product based on the joint thermal- and near-infrared retrieval. We use version 9 data with a resolution of 1x1°. A detailed description of the data set including information on the retrieval algorithm and the available products are provided in the User Guide by the MOPITT Algorithm Development Team (2022) and in Deeter et al. (2022). An a priori CO profile is required, which is generated with the CAM-Chem model based on monthly climatological data from 2000 to 2009. The a priori is spatially and monthly variable but has no interannual variability. Based on MOPITT radiance and MODIS (Moderate Resolution Imaging Spectroradiometer) cloud detection, only cloud-free retrievals are processed for the Level 3 product. Observations with low signal-to-noise ratios (SNR) are discarded (Average radiance SNR < 1000 for thermal and < 400 for near infrared retrieval). The averaging kernel provides information on the altitude sensitivity of the satellite retrieval. The thermal retrieval is most sensitive between 400 and 600 hPa (approximately 4–7 km altitude), whereas the multi-spectral CO product used in this study shows some additional sensitivity to the lower troposphere (Worden et al., 2010). However, the datasets do not show significant differences in CO changes over time.

2.1.5 IASI Satellite Observations

We use carbon monoxide retrievals from the IASI instrument onboard the ESA's MetOp-B satellite from 2014 to 2024, as well as the MetOp-A satellite from 2008 to 2019. The satellites have a local overpass time of 9:30 AM and 9:30 PM. IASI measures the spectral radiance using Fourier Transform Spectrometry (George et al., 2015). We use the monthly daytime Level 3 Metop-A and Metop-B products from IASI with a resolution of 1x1° based on thermal-infrared retrieval. The FORLI (Fast Optimal/Operational Retrievals on Layers for IASI) algorithm v20151001 (Hurtmans et al., 2012) is used to obtain the CO profiles. The a priori consists of a single spatially and temporally invariant CO profile based on assimilated model, satellite and MOZAIC aircraft data. Further information on the IASI CO retrieval can be found in Astoreca et al. (2016) and Clerbaux et al. (2009). Similar to the MOPITT CO product, the sensitivity of the IASI retrieval is largest in the mid troposphere.

2.1.6 OMI Satellite Observations

Formaldeyhde (HCHO) and nitrogen dioxide (NO_2) are measured by the Ozone Monitoring Instrument (OMI) onboard the NASA's Aura satellite with an overpass time of 1:45 AM and 1:45 PM. We use the total column daily gridded Level 3 product with a resolution of 0.1x0.1° for HCHO (OMHCHOd) and 0.25x0.25° for NO_2 (OMNO2d) from the years 2005 to 2021. For the HCHO Level 3 data processing, retrievals with high cloud cover, high solar zenith angle (SZA) and those impacted by the OMI row anomaly are discarded. Similarly, the NO_2 retrievals are filtered for cloud fraction and SZA. We use versions V3 and V4 for HCHO, which we additionally filter for values below -8e15 and above 7e16 molecules cm^{-2} in accordance with Johnson et al. (2024). We investigate version V3 for NO_2. For both species, we use the sample weight representing the weight

https://doi.org/10.5194/egusphere-2026-5476
Preprint. Discussion started: 11 September 2026

of each Level 2 pixel for the Level 3 product generation to calculate temporal and spatial means. Further details on the OMI instrument and the NO_2 and HCHO column retrievals are provided by the OMI Nitrogen Dioxide Algorithm Team (2019) and Gonzalez Abad and Sun (2019), respectively.

2.2 Model Simulations

GEOS-Chem is a global chemistry transport model driven by assimilated meteorology from the NASA Global Modeling Assimilation Office (GMAO) (GEOS-Chem, 2026; Bey et al., 2001). We use GEOS-Chem Classic version 14.4.3 (GCClassic 14.4.3, The International GEOS-Chem User Community (2024)) with MERRA-2 meteorological inputs to simulate mixing ratios of carbon monoxide and related trace gases between 2000 and 2022 (preceded by an 18 month spin-up) with a horizontal resolution of 2°x2.5°, a vertical resolution of 47 layers and a temporal resolution of 600 s for transport and 1200 s for chemistry. The chemical mechanism includes reaction rate coefficients as recommended by JPL and IUPAC (Bates et al., 2024). The calculation of photolysis frequencies is based on the Cloud-J model by Prather (2015). Emissions are controlled by the Harmonized Emissions Component (HEMCO) version 3.9.3 (Keller et al., 2014; Lin et al., 2021). All emissions are year-specific unless otherwise stated. We use monthly anthropogenic emissions of the Community Earth atmospheric Data System (CEDS) (version v_2021_04_21) (Hoesly et al., 2018) and monthly biomass burning emissions from the Global Fire Emissions Database version 4.1 (GFED4s) (van der Werf et al., 2017). CEDS emissions for GEOS-Chem 14.4.3 are available up to 2019. To account for emission changes in more recent years, we scale the v2021 NO and CO emissions from 2019 to 2020-2022 by the changes observed in the v2025 CEDS emissions, which are available up to the present. We perform the scaling by sector and grid (each grid box individually), except for shipping emissions, which we scale by a constant factor for the SH and NH due to large uncertainties from changes in the ship track location between the versions. Methane surface mixing ratios from 2000 to 2022 follow the marine boundary layer reference by the NOAA GML (Lan, 2024; Lan et al., 2025) interpolated to a horizontal resolution of 1°x1° and a temporal resolution of 1 month. We use offline, year-specific natural emissions, including hourly biogenic volatile organic compounds (BVOC) from the Model of Emissions of Gases and Aerosols from Nature (MEGAN), hourly soil NO_x emissions (Hudman et al., 2012) and 3-hourly lightning NO_x emissions (Murray et al., 2012). All spatial averages presented are weighted by area.

We run several sensitivity tests to characterize the impact of changes in anthropogenic and natural CO emissions, as well as precursors emissions and temperature on tropospheric CO mixing ratios. We summarize the sensitivity studies in Table 1. We carry out all sensitivity tests for the year 2018 with a 1-year spin-up period. To investigate the effect of enhanced OH, we introduce an additional OH source by adding an artificial OH-producing reaction to the chemical mechanism for simulation #7 OH_{all}: CO + OH → CO + 2OH with k=0.05*k(CO+OH). Simulation #12 T_{all} explores the isolated response of temperature on rate coefficients and the resulting trace gas abundance. While it does not represent a realistic scenario, as temperature increases are usually accompanied by other changes, such as humidity, that are not interactive in GEOS-Chem, it provides an isolated assessment of the impact of temperature on CO levels.

https://doi.org/10.5194/egusphere-2026-5476
Preprint. Discussion started: 11 September 2026

Table 1. Overview of the sensitivity studies performed with GEOS-Chem in the scope of this study. We ran all simulations for 2018 with a 1-year spin-up.

#	Simulation name	Description
1	CO_{BL}	Baseline run (2018)
2	CO_{all}	25% increase in all CO emissions
3	CO_{anthro}	25% increase in anthropogenic CO (CEDS emission inventory)
4	CO_{BB}	25% increase in biomass burning CO (GFED emissions inventory)
5	NO_{all}	25% increase in all NO emissions
6	CO_{all} & NO_{all}	25% increase in all CO and all NO emissions (2 & 5)
7	OH_{all}	5% increase in the tropospheric mass-weighted mean OH concentration (artificial OH source)
8	$Isoprene_{all}$	25% increase in all Isoprene emissions
9	$CH_{4\ surface}$	10% increase in surface CH_4 mixing ratios
10	$Cl_{2\ ocean}$	Additional emission of 10Tg Cl_2 spread equally over all ocean surfaces
11	$Cl_{2\ ocean}$ & $CH_{4\ surface}$	10Tg Cl_2 & 10% increase in CH_4 (9 & 10)
12	T_{all}	1°C increase in atmospheric temperature, surface temperature and 2m temperature

2.3 Emission inventories

We compare the emissions of CO and NO in the Southern Hemisphere as estimated in different emission inventories. These include anthropogenic emissions from CEDS. We use emissions from the versions v2021 (as processed for GEOS-Chem), v2024, and v2025 with a resolution of 0.5x0.5° (Joint Global Change Research Institute, 2025b, c). A detailed description of the emission inventory and the version history is provided by the Joint Global Change Research Institute (2025a). We further include anthropogenic emissions from the Copernicus Atmosphere Monitoring Service (CAMS) in versions CAMS-GLOB-ANT-V5.3 and CAMS-GLOB-ANT-V6.2, as provided by the Emissions of Atmospheric Compounds and Compilation of Ancillary Data (ECCAD) system with a resolution of 0.1x0.1° (Copernicus Atmosphere Monitoring Service, 2024, 2026). The CAMS anthropogenic emission inventory is described in detail in Soulie et al. (2024). We investigate biomass burning emissions of CO and NO from GFED4s with a resolution of 0.25x0.25° (van der Werf et al., 2017). We compare these with fire emissions from the Global Fire Assimilation System (GFAS), version v1.2, obtained from the Copernicus Atmosphere Monitoring Service (2022) with a resolution of 0.1x0.1° (Kaiser et al., 2012).

https://doi.org/10.5194/egusphere-2026-5476
Preprint. Discussion started: 11 September 2026

3 Results and Discussion

3.1 Observations

In this section, we investigate changes in tropospheric carbon monoxide in the remote Southern Hemisphere between 2008 and 2022 (or according to data coverage, Table S1) based on surface measurements, aircraft observations and satellite retrievals. We compare GEOS-Chem model simulations of CO along the aircraft flight tracks and at the surface.

3.1.1 Surface observations

We investigate the possibility of a trend in the SH surface CO based on NOAA and CSIRO measurement records at 12 sites over 14 years in the southern extratropics (Figure 2). This period (2008 to 2022) corresponds to the strong upward trend in observed CH_4 levels. Figure 3 presents the observed SH surface CO product at (a) the CSIRO sites (light blue circles) and (b) the NOAA sites (dark blue squares). Simulated CO at these same sites is shown in gray. The lines represent linear fits of the yearly values between 2008 and 2022. We exclude the 2020 outlier from the fit to avoid a high bias of the trend. The elevated CO in 2020 is likely due to enhanced wildfire emissions from the 2019/2020 Australian bush fires (Pope et al., 2021), with a possible contribution of reduced OH as an outcome of the COVID-19 emission reductions (Heald et al., 2026). Additionally, enhanced isoprene in 2020 as reported by Yoon et al. (2025) could deplete OH and therefore increase the CO lifetime.

The observed CSIRO composite (Figure 3 (a)) shows an increase of CO by 6.4 % (from around 50 ppbv to 53 ppbv) between 2008 and 2022, which is significant (p-value=0.004). The simulated CO at the CSIRO sites exhibits a similar significant increase by 5.8 % (p-value=0.046). In contrast, the observed NOAA composite does not show any significant change of CO between 2008 and 2022. Simulated CO at the NOAA sites increases significantly by 5.7 % (p-value=0.032), which is similar to the increase observed at the CSIRO sites. Given the trend analysis is based on a short period of time, we verify that the model-observation comparison is not unduly influenced by any given year. We perform 10,000 residual bootstrap iterations with replacement for the linear fitting of the yearly averages (for each iteration a random sample of the residuals added to the predicted values is fitted, maintaining a constant sample size equal to the number of years). The resulting histograms, shown in Figure 3 (c) for CSIRO sites and (d) for NOAA sites demonstrate the robustness of the trend similarity and difference, respectively, between simulations and observations.

We show the changes in the annual mean CO at all sites in Figure S2 of the Supplement, which highlights that the individual trends are similar to the composite trends in Figure 3. Significant positive trends of 6–7 % are observed at all CSIRO sites, while the NOAA sites show a roughly equal number of up- and downward trends, which are insignificant (p-value>0.05). This difference between CSIRO and NOAA observed CO trends is equally observed at the sites with co-located measurements (CGO and SPO). We can therefore exclude the geographic difference of the sites as a reason for the trend difference. At the site CGO (Kennaook/Cape Grim), continuous CO measurements (calibrated using the CSIRO2020 calibration scale) are available from the station, which is part of the AGAGE (Advanced Global Atmospheric Gases Experiment) network. At this site, CO mixing ratios increased (statistically significant) by 7.1 % between 2008 and 2022. The simulated CO trends are positive at all sites. At the majority of sites, the model underestimates the CO observations by approximately 10 %. This is likely the result

https://doi.org/10.5194/egusphere-2026-5476
Preprint. Discussion started: 11 September 2026

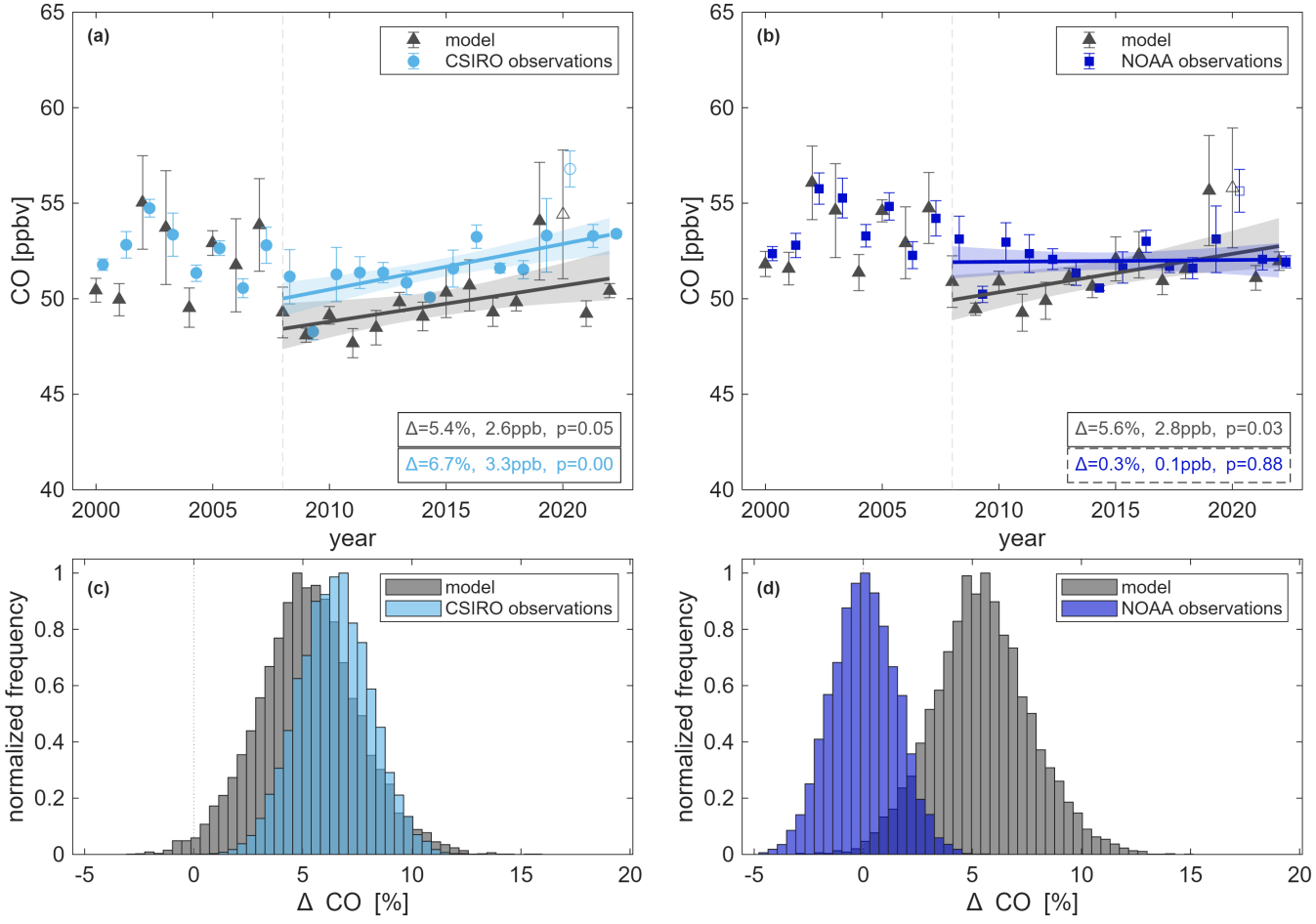

Figure 3. Observation-based (blue) and GEOS-Chem simulated (gray) annual mean CO at **(a)** the CSIRO sites and **(b)** the NOAA sites in the Southern Hemisphere extratropics between 2000 and 2022. Symbols show yearly averages of the deseasonalized data following NOAA GML (2025b) and error bars highlight the uncertainty (root mean square value of the 1σ standard deviation from the yearly averaging of the deaseasonalized data at the individual sites). The lines indicate the linear fit between 2008 and 2022 and the errorshades show the 95 % residual-bootstrap confidence interval. The boxes show the absolute and relative changes of CO over this time period. Solid boxes indicate significant (p-value<0.05) and dashed boxes insignificant fits (p-value>0.05). We do not include the 2020 values (shown as open symbols) in the fit to avoid a high bias (see Section 3.1.1). **(c)/(d)** Normalized frequency distribution of the changes in CO levels at (c) CSIRO and (d) NOAA sites between 2008 and 2022 based on 10,000 bootstrap iterations (with replacement) of the annual trends in panel (a) and (b).

of a known high OH bias (Naik et al., 2013; Zhao et al., 2023; Yang et al., 2025); however, uncertainties in anthropogenic CO emissions (see Section 3.2), isoprene emissions (Yoon et al., 2025), or biomass burning emissions (see Section 3.2) may also contribute. At BHD, CGO and CPT the model overestimates observed CO, which is due to the anthropogenic impact of nearby sources (these sites are less remote than the other sites). While the observational data are filtered for background

https://doi.org/10.5194/egusphere-2026-5476
Preprint. Discussion started: 11 September 2026

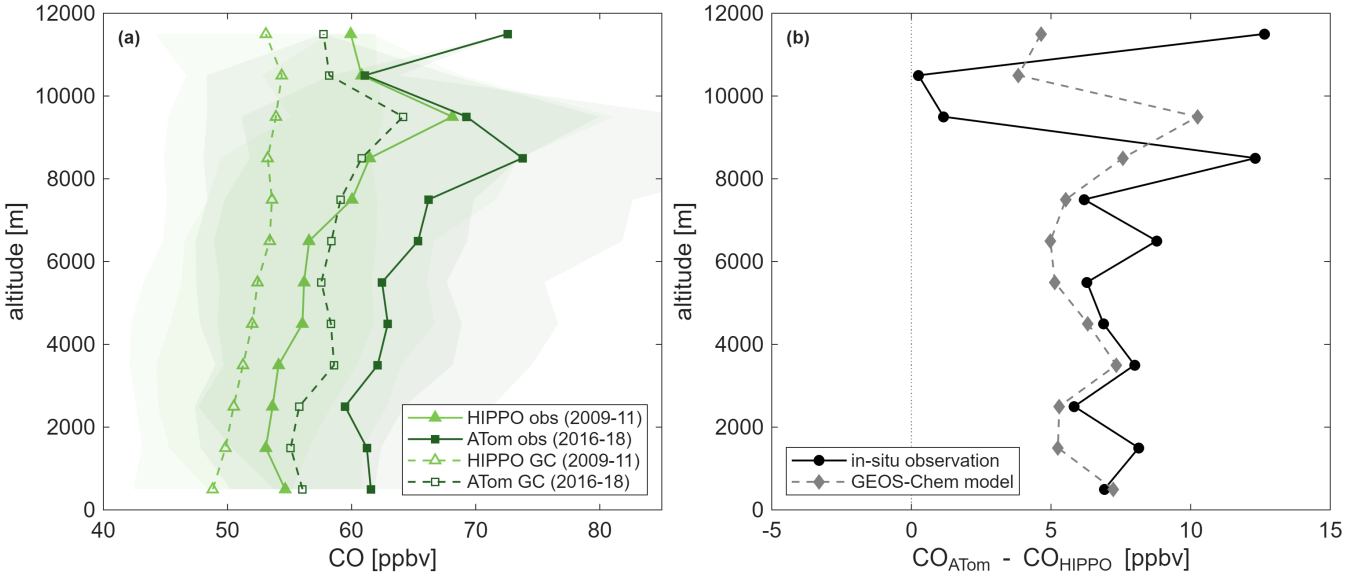

Figure 4. (a) Mean vertical profiles of CO during the HIPPO (2009–2011, light green triangles) and the ATom campaigns (2016–2018, dark green squares). In-situ observations are shown by filled symbols and solid lines; GEOS-Chem (GC) simulated mixing ratios are presented by open symbols and dashed lines. Symbols represent averages binned to 1 km altitude and the shading indicates the 1σ standard deviation around the mean. **(b)** Vertical profile of the mean difference between ATom and HIPPO CO. Observations are shown in gray and model results are shown in green.

conditions based on wind speed and direction, the simulated data have a monthly resolution and thus include air masses from all directions.

The observed trends inferred from the CSIRO and NOAA sites are not consistent. A particular challenge with regards to CO observations is the stability of CO calibration standards, which are prone to drifts over time and need to be corrected. The calibration scale for the NOAA CO flask measurements was recently updated from WMO CO X2014A to WMO CO X2025 (NOAA Global Monitoring Laboratory, 2026), whereas the CSIRO observations rely on the independent CSIRO2020 scale. Both scales face similar challenges related to the uncertainties described in primary CO standards. The NOAA CO data calibrated on the previous WMO CO X2014A scale shows a significant positive trend (consistent with the trend shown at the CSIRO sites), highlighting the key impact of calibration on data inter-comparison and interpretation and the continued need to improve current calibration scales.

3.1.2 Aircraft observations

Figure 4 shows the mean vertical profile of carbon monoxide measurements from the southern extratropical legs of the HIPPO and ATom campaigns (flight tracks shown in Figure 2). The mean observed vertical profiles are shown in Figure 4(a) with filled symbols and solid lines and the GEOS-Chem simulations sampled along the flight tracks are shown by open symbols

https://doi.org/10.5194/egusphere-2026-5476
Preprint. Discussion started: 11 September 2026

and dashed lines. CO does not exhibit a strong altitude dependence, as expected over the remote oceans, given the limited local primary sources. During the HIPPO campaigns between 2009 and 2011, CO mixing ratios averaged 55–60 ppbv. In comparison, during the ATom campaigns between 2016 and 2018 CO levels were ∼10 % higher. This increase (4(b)) is well-captured by the GEOS-Chem simulations sampled along the flight tracks. The zonal average of observed CO levels during HIPPO, ATom and the difference (Figure S3) highlights that the increase in CO is predominantly limited to the southern extratropics. The difference persists across all seasons (Figure S4). While Figure 4 compares observations at similar longitudes, the difference between both campaigns remains across all southern extratropical longitudes for MAM, JJA and SON. In contrast for DJF, the difference between ATom and HIPPO only appears when isolating the longitudes where both datasets overlap.

The largest difference in measured CO occurs in SON, which represents the peak biomass burning season in the Southern Hemisphere. We also observe a significant difference in black carbon between HIPPO and ATom (only) in SON, suggesting that some of the CO difference in SON is due to differences in fire contribution. This difference is likely super-imposed on the photochemically produced CO differences seen throughout the rest of the year. Neither the HIPPO nor the ATom campaigns took place during years of peak fire activity in the Southern Hemisphere, indicating that biomass burning is not the primary driver of the overall increase in CO (Chen et al. (2023), see Section 3.2). While GEOS-Chem represents the increase of CO from HIPPO to ATom well, it underestimates CO levels during both campaigns by approximately 10 % throughout the entire troposphere as previously discussed (Section 3.1.1).

Similar to the surface observations, the calibration of the aircraft CO measurements introduces additional uncertainty for the inter-comparison of HIPPO and ATom in-situ CO observations. The calibration of the HIPPO CO data is based on the WMO X2004 scale, while the ATom CO data is on the WMO X2014A calibration scale. To verify that the observed increase of CO from HIPPO to ATom is not primarily due to the use of different calibration scales, we compare the CO observations from the Programmable Flask Package (PFP), which have been updated to the WMO X2025 scale for both aircraft campaigns. While the PFP data suffer from statistical limitations due to a low sampling frequency, resulting in uneven coverage across altitude and seasons, Figures S5 and S6 show that the difference in CO levels between HIPPO and ATom persists across all seasons with the PFPs on the WMO X2025 scale. The annual average change at all altitudes between ATom and HIPPO in the PFP data is 9.7 % compared to 12.4 % for the in-situ high frequency observations. We therefore conclude that the observed difference is caused by atmospheric changes rather than a drift in calibration standards.

3.1.3 Satellite observations

Figure 5(a) and (b) present the changes of column CO as observed by the MOPITT (red) and the IASI (orange) instruments, respectively, over the southern extratropics. Average MOPITT CO columns are mostly constant in the southern extratropics over the past 15 years. In contrast, average IASI Metop-B CO columns exhibit a 4 % increase between 2014 and 2023, which is marginally significant (p-value=0.07); however, we note that the statistical evaluation of a small number of years is limited. The Metop-A and Metop-B columns overlap between 2014 and 2019 and show close agreement, which is in line with findings by García et al. (2016). The IASI Metop-A CO column averages from 2008 onward show a slightly smaller, but overall similar increase, which is not significant (Δ=2.3 %, p-value=0.38).

https://doi.org/10.5194/egusphere-2026-5476
Preprint. Discussion started: 11 September 2026

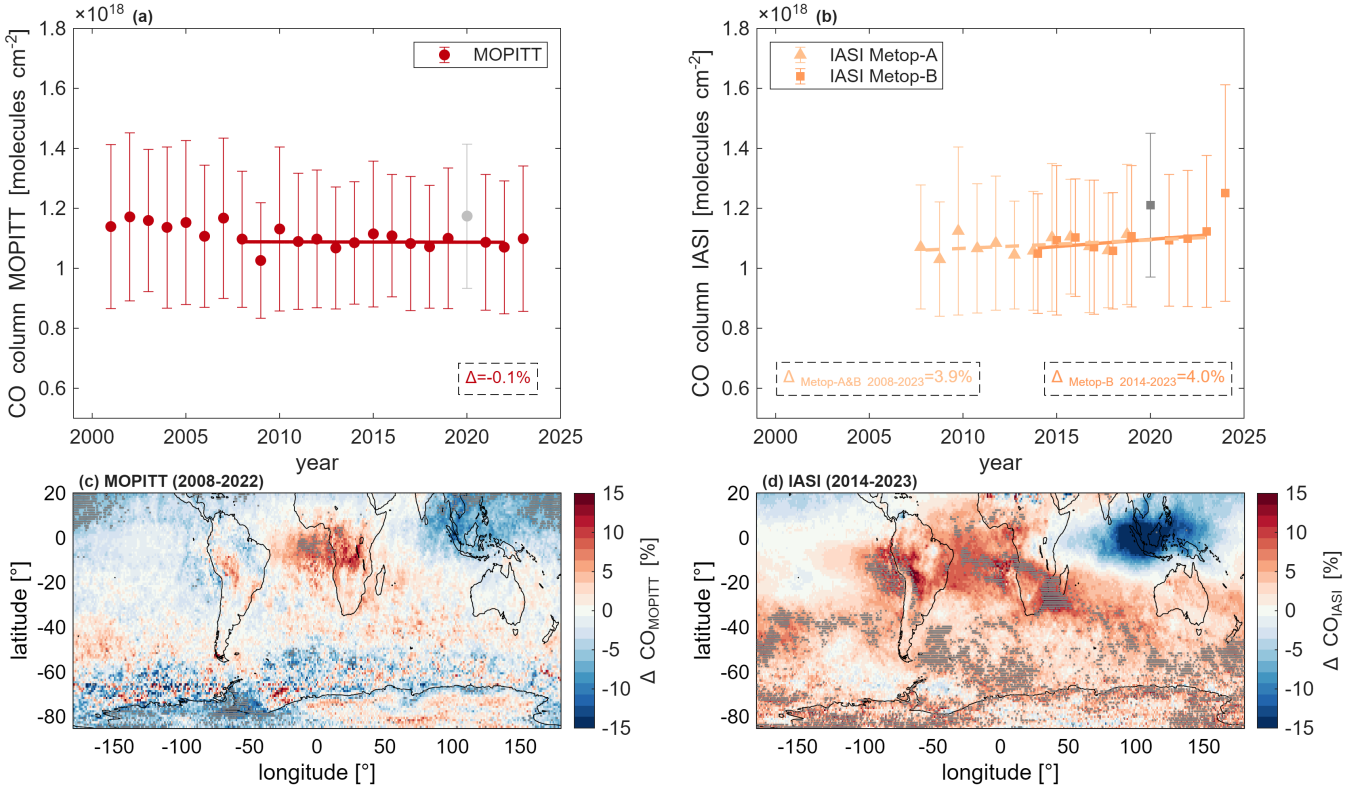

Figure 5. CO column trends in the southern extratropics. **(a)&(b)** Changes of column CO in the southern extratropics (a) between 2001 and 2022 as inferred from MOPITT (red) and (b) as measured by IASI Metop-A (2008–2019, orange open symbols) and Metop-B (2014–2024, orange filled symbols). Circles and squares show yearly averages and error bars represent the 1σ standard deviation of the averaging. The solid lines indicate the linear fit between 2008 and 2022 for MOPITT and between 2014 and 2023 for IASI Metop-B. The dashed line represents the linear fit between 2008 and 2023 for IASI with combined Metop-A (2008–2013) and Metop-B (2014–2023) data. The boxes show the relative changes of CO over this time period. Neither fit is significant (p-value$_{\mathrm{MOPITT}}$=0.95, p-value$_{\mathrm{IASIMetop-B}}$=0.07 and p-value$_{\mathrm{IASIMetop-A\&B}}$=0.08). **(c)&(d)** Relative changes in CO columns for MOPITT (c) and IASI (d). Dots indicate significant changes (p-value$<$0.05 and $R^2>0.4$).

Figure 5(c) and (d) show the geographical overview of the trends retrieved from MOPITT and Metop-B IASI, respectively. Blue colors show decreases and red colors show increases of the CO column. Southern Hemisphere source regions are characterized by large, but statistically insignificant, changes in CO, consistently observed with both MOPITT and IASI. However, the satellites differ in the trend in extratropical CO. MOPITT CO columns are characterized by mostly insignificant decreases throughout the southern extratropics. In contrast, IASI Metop-B CO columns show predominantly positive changes, however only a small number of grid cell trends are significant. South of 30°S latitude ∼90 % of grid cells show increases of 3–4 % of which ∼20 % are significant.

https://doi.org/10.5194/egusphere-2026-5476
Preprint. Discussion started: 11 September 2026

The analysis of the two satellite retrievals is inconclusive with regards to whether there has been a trend in CO observed in the southern extratropics. While IASI columns overall support the CSIRO surface observations, changes in MOPITT columns align with the observations at the NOAA surface sites. However, both datasets provide mostly insignificant results. We do not observe a significant change in the trend when restricting the analysis of MOPITT data to the time period of IASI data availability. The trends are consistent across each season. Differences between MOPITT and IASI CO can result from a varying choice of CO a priori in the retrievals. However, there is no time variation in the a priori in either product, which could contribute to the observed trends. Satellite data can further be impacted by the cloud cover, however the daily overpass times of both satellites are similar, minimizing this effect. MOPITT CO trends in the Southern Hemisphere were previously investigated by Hedelius et al. (2021), who reported small increases for the two periods 2009–2013 and 2013–2017. Similarly, we find (insignificant) increases of MOPITT CO columns over these periods, which are strongly driven by individual years, e.g. low CO in 2009. Deeter et al. (2022) reported drifts in the V9 total column combined retrievals of -3.16e14 molecules cm^{-2} $year^{-1}$, which sum up to <0.5 % over the observed time period and are therefore unlikely to cause the observed difference between the two satellite products. Further research is needed to understand the reasons for the discrepancies in CO columns derived from MOPITT and IASI in the southern extratropics.

In addition, space-based measurements are available for HCHO - an intermediate product in CO formation - from the satellite-based OMI instrument. However, observations are close to the detection limit over the remote Southern Hemisphere and different data versions provide inconsistent results. The daily Level 3 product in version V3 suggests an increase of around 13 % between 2008 and 2021, whereas the updated V4 OMI HCHO data (more reliable after 2014) exhibit a decline by around 13 % over the same time period (Figure S7). The TROPOspheric Monitoring Instrument TROPOMI with a lower detection limit, could provide more reliable information on tropospheric HCHO. However, the current data availability (2019–2024) is insufficient to conduct a meaningful trend analysis.

3.2 Global Model Simulations

In this section, we investigate the drivers of the changes in CO simulated with GEOS-Chem between 2008 and 2022. In contrast to the previous section, where we examined model output in comparison with co-located observations, here we focus on widespread model trends throughout the southern extratropics.

Figure 6 shows the trend in simulated carbon monoxide in the southern extratropics at the surface (Figure 6(a)) and in the tropospheric column (Figure 6(b)). Both the surface mixing ratios and the column concentrations exhibit significant CO increases (p-value<0.05) of 6.6 % from 2008 to 2022. The increase is persistent throughout all seasons (Figure S8). The years 2019 and 2020 show particularly high levels of CO, which is most pronounced during DJF (for 2019 and 2020) and SON (for 2019), largely due to enhanced wildfire emissions from the 2019/2020 Australian bush fires and the 2019 peat fires in South East Asia. In contrast to the upward trend of CO from 2008 onward, simulated CO was mostly constant or declined slightly between 2000 and 2008. The earlier trend is not significant and changes are dominated by the year-to-year variability. Figure 6(c) and (d) show the geographical changes of CO between 2008 and 2022 at the surface and throughout the column, respectively. The panels show that the CO increase is spatially consistent throughout the southern extratropical troposphere

https://doi.org/10.5194/egusphere-2026-5476
Preprint. Discussion started: 11 September 2026

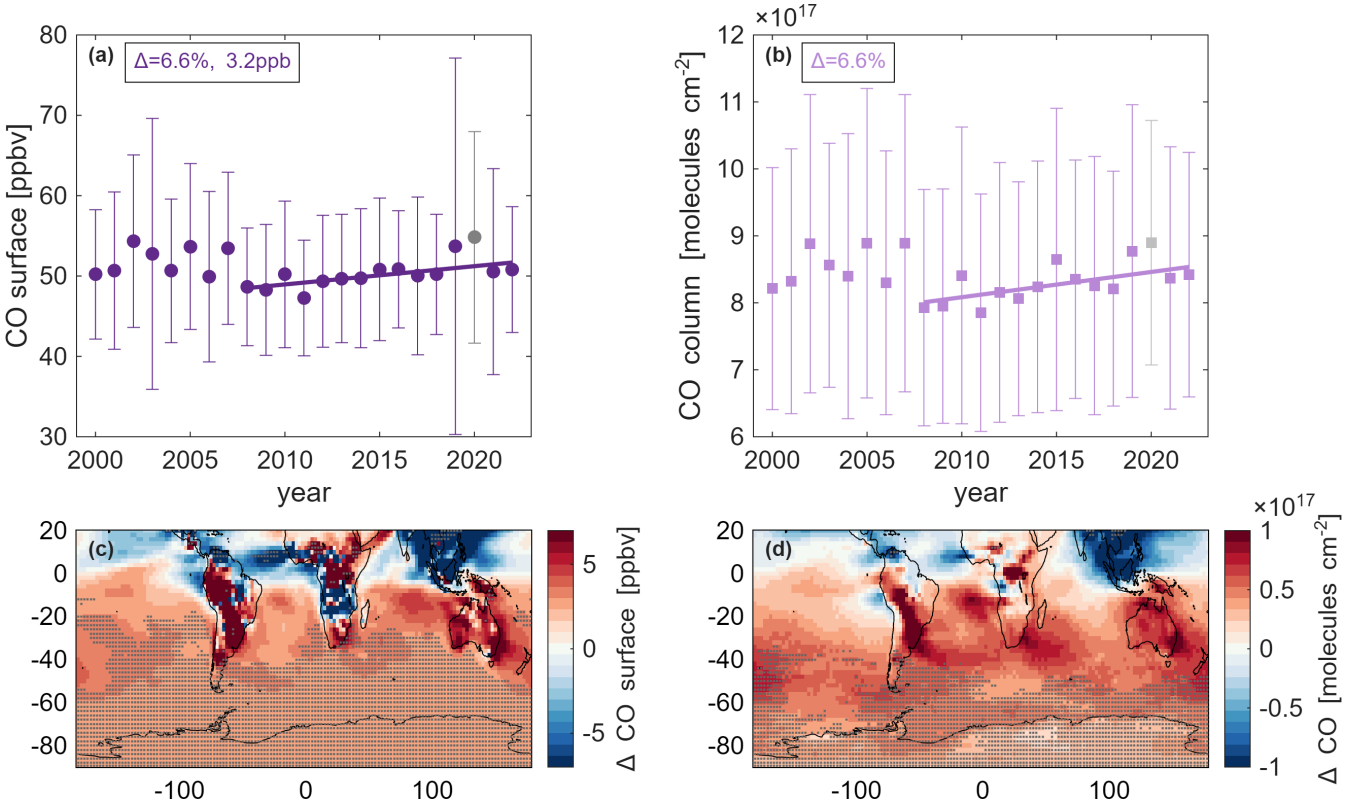

Figure 6. (a)&(b) Changes of simulated CO between 2000 and 2022 in the southern extratropics (LAT $< -30°$) as (a) mixing ratios at the surface (dark blue) and (b) column concentrations throughout the troposphere (light blue). Circles and squares show yearly averages and error bars represent the 1σ standard deviation of the averaging. The solid lines indicate the linear fit between 2008 and 2022 and the boxes show the absolute and relative changes of CO over this time period. Both fits are significant (p-value$<$0.05). We do not include the 2020 values (shown as gray symbols) as described earlier. **(c)&(d)** Changes in simulated CO mixing ratios between 2008 and 2022 at the surface (c) and in the tropospheric column (d). Dots indicate significant changes (p-value$<$0.05 and $R^2>0.4$).

with surface increases of around 3–4 ppbv over 14 years. The trends are predominantly significant over the Southern and remote extratropical Oceans, as well as Antarctica, whereas simulated changes over continental regions in the SH are mostly insignificant due to large inter-annual variability.

While we focus on CO mixing ratios in the remote SH, changes thereof can originate from anywhere within the hemisphere due to the similar timescales of CO lifetime and intra-hemispheric mixing. We therefore investigate photochemical processes and emissions in the entire Southern Hemisphere as potential drivers of the simulated CO trend.

Figure 7(a) shows the average monthly contribution of CO emissions and photochemical production to the total CO source in the SH, from the 23-year GEOS-Chem simulation. The photochemical formation of CO dominates the overall source throughout the year with a seasonal maximum in February and a minimum in August. Annually, ∼60 % of secondary CO is produced

https://doi.org/10.5194/egusphere-2026-5476
Preprint. Discussion started: 11 September 2026

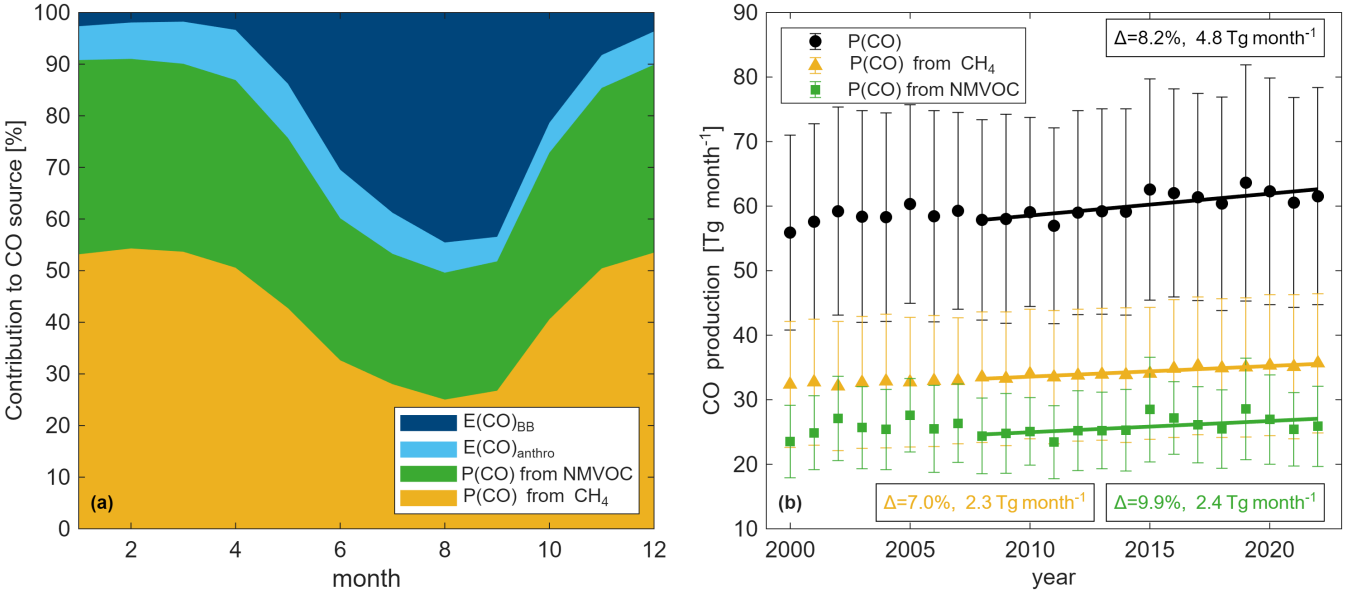

Figure 7. (a) Average (2000–2022) monthly contribution of primary CO emissions and photochemical production to the overall CO source in the Southern Hemisphere based on GEOS-Chem simulations using the GFED4s and CEDS v2021 data. (b) Changes of the CO production terms in the Southern Hemisphere between 2000 and 2022. Black colors show total CO production, yellow colors indicate CO production from CH_4 and green colors represent CO production from NMVOCs. Symbols show yearly averages and error bars represent the 1σ standard deviation of the averaging. The lines indicate the linear fit between 2008 and 2022 and the boxes show the changes over this time period. All fits are significant (p-value$<$0.05).

from CH_4 and ∼40 % from NMVOC. The production of CO is mainly driven by the availability of sunlight, which peaks during SH summer (DJF). In contrast, emissions are largely controlled by the biomass burning season with peak wildfire emissions between June and October (more than 85 % of wildfire CO is emitted during these months). Anthropogenic CO emissions are generally constant throughout the year. The annual average source of CO in the SH consists of ∼40 % CH_4 oxidation, ∼30 % NMVOC oxidation, ∼20 % biomass burning emissions and ∼10 % anthropogenic emissions.

Figure 7(b) shows simulated tropospheric CO production in the SH between 2000 and 2022. The total CO production (black) increases by around 8 % from 58 Tg month^{-1} in 2008 to 63 Tg month^{-1} in 2022. Considering that photochemical production contributes approximately 70-80 % to the overall CO source (Figure 7(a)), this P(CO) increase explains the increase in total simulated CO shown in Figure 6. It includes both enhancements in the production of CO from CH_4 and NMVOCs as shown in yellow and green, respectively. The simulated production of CO does not change significantly between 2000 and 2008. The simulated HCHO column increases by 7 % in the southern extratropics between 2008 and 2022; as an important intermediate in the CO production pathway it reflects the increase in both CH_4 and NMVOC oxidation.

Figure 8 shows that both the plateau in P(CO) from 2000–2008 and the increase from 2008–2022 reflect the CO precursor trends. Simulated SH extratropical surface CH_4 averages (which follows the observations of the surface flask network) are

https://doi.org/10.5194/egusphere-2026-5476
Preprint. Discussion started: 11 September 2026

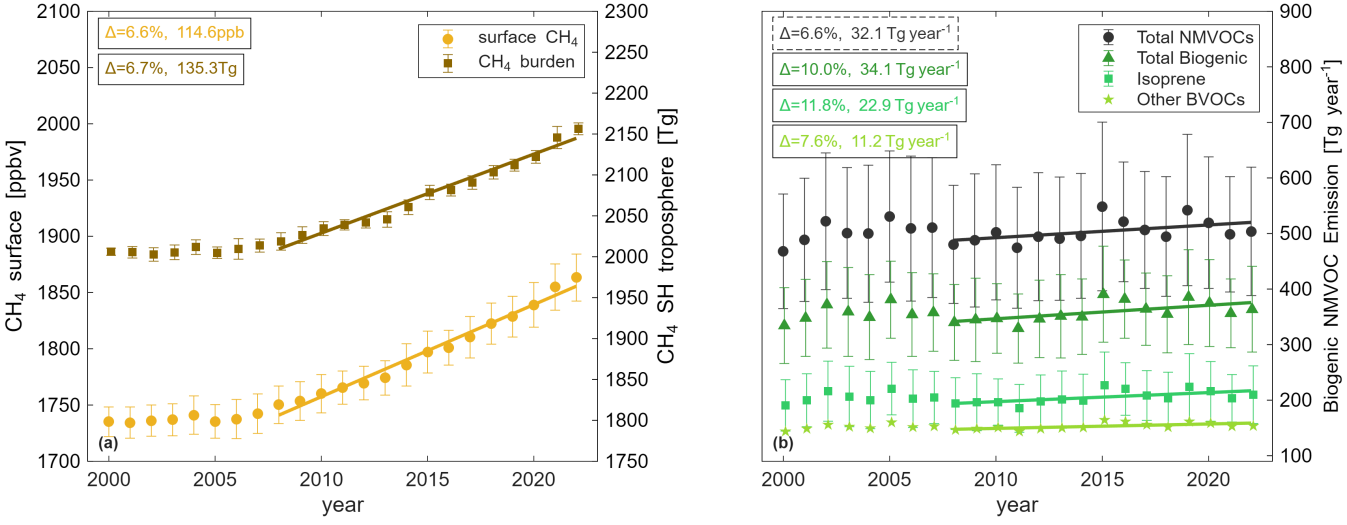

Figure 8. Changes of CO precursors between 2000 and 2022 based on GEOS-Chem simulations. **(a)** Surface CH_4 mixing ratios in the southern extratropics (yellow circles) and tropospheric CH_4 burden in the SH (brown squares); **(b)** biogenic NMVOC emissions in the SH. Symbols show yearly averages and error bars represent the 1σ standard deviation of the averaging. The lines indicate the linear fit between 2008 and 2022 and the boxes show the changes over this time period. Solid boxes indicate significant (p-value$<$0.05) and dashed boxes insignificant trends (p-value$\geq$0.05).

mostly constant for several years at the beginning of the century between 2000 and 2007 with values around 1735 ppbv and then rapidly increases to 1860 ppbv in 2022. This behavior is well known in the current literature; however, the reason for it has not been fully resolved (Turner et al., 2019; Saunois et al., 2020; Skeie et al., 2023). Both surface CH_4 and the SH tropospheric CH_4 burden increase by $\sim$6.5 % between 2008 and 2022. The CH_4 increase since 2008 explains around 90 % of the observed enhancement in the CO production term from CH_4 (Figure 7(b)) and approximately 50 % of the overall CO increase.

CO can also be produced photochemically via the oxidation of NMVOCs. Biogenic VOCs contribute over 70 % of this photochemical NMVOC source (300-400 Tg yr^{-1}) in the SH, and isoprene, which is primarily emitted from deciduous vegetation, dominates this (60 %). Bicyclic monoterpenes and methanol contribute $\sim$10 % each, acetone and mono-/acyclic monoterpenes each contribute $\sim$5 %, and, "Other BVOCs", including acetaldehyde, ethylene, ethanol, limonene and C3 alkanes, make up the remaining $\sim$10 % (Figure S9). While the isoprene lifetime is of the order of hours and long-range transport (e.g. from the tropical forest to the remote Southern Hemisphere) is negligible, it can be oxidized and form CO locally, which can then be transported throughout the SH. Figure 8(b) shows the changes of total NMVOC emissions in GEOS-Chem in black and biogenic NMVOC emissions in shades of green between 2000 and 2022. The contribution and trends of other NMVOC sectors are shown in Figure S10. Total NMVOC emissions increase by $\sim$30–35 Tg between 2008 and 2022. The trend is marginally significant (p-value=0.06) and can be attributed to significant increases in biogenic NMVOC emissions (dark green triangles), and particularly to isoprene (light green squares). Biogenic NMVOC emissions therefore drive the increase in CO production

https://doi.org/10.5194/egusphere-2026-5476
Preprint. Discussion started: 11 September 2026

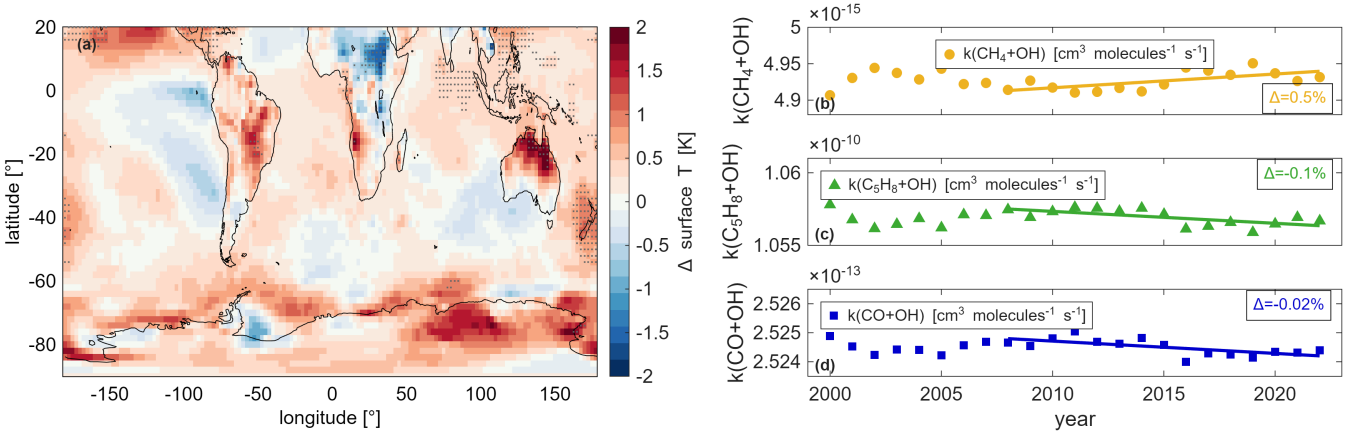

Figure 9. (a) Changes of surface temperature between 2008 and 2022. Dots indicate significant changes (p-value$<$0.05 and $R^2>0.3$); **(b)-(d)** Changes of the rate constants of **(b)** CH_4 + OH, **(c)** C_5H_8 + OH and **(d)** CO + OH in the Southern Hemisphere.

from NMVOCs as shown in Figure 7(b), which in turn contribute to the overall enhancement in the photochemical production of CO by ∼40–45 %.

Biogenic NMVOC emissions generally increase with increasing temperature (typically up to a threshold) (Sharkey and Singsaas, 1995; Guenther et al., 2006). Surface temperature increased across the Southern Hemisphere by around 0.3 °C between 2008 and 2022 in the MERRA2 meteorological reanalysis (Figure 9(a)). These temperature changes in GEOS-Chem translate into changes in BVOC emissions (Figure S11(a)). Isoprene emission increases occur predominantly in tropical regions, which also feature temperature enhancements, including South America, Australia and South East Asia. In contrast, central Africa shows small decreases in isoprene emissions coinciding with temperature decreases.

In addition to the effect of temperature on biogenic emissions, temperature also impacts CO formation via temperature-dependent kinetics. Figure 9(b)-(d) show the changes of the rate coefficients of the CO production and loss terms since 2000. The rate coefficient k(CH_4+OH) in Figure 9(b) exhibits Arrhenius behavior and increases by 0.5 % across the Southern Hemisphere between 2008 and 2022. The rate coefficients k(C_5H_8+OH) and k(CO+OH) show a negative (but much smaller) temperature correlation (anti-Arrhenius behavior). Increasing temperatures therefore enhance the dominant production term of CO via CH_4, while weakening the loss of CO via OH. The increases in temperature contribute around 10 % to the CO increase from CH_4 oxidation and ∼5 % to the overall CO increase between 2008 and 2022 (Figure S12).

A number of additional sources and sinks can influence CO levels as highlighted in Figure 1, but do not contribute to the simulated model trend from 2008 to 2022. These include anthropogenic and biomass burning emissions of CO, emissions of NO, and levels of tropospheric oxidants. Figure 10(a) presents an overview of early 21^{st} century trends of CO emissions in the Southern Hemisphere based on different emission inventories. SH emissions are dominated by biomass burning (red color scale) rather than anthropogenic sources (blue and green colors). The GFED4s (used to drive the GEOS-Chem simulations in this study) and the GFAS v1.2 biomass burning emission estimates show a statistically insignificant downward tendency (10-

https://doi.org/10.5194/egusphere-2026-5476
Preprint. Discussion started: 11 September 2026

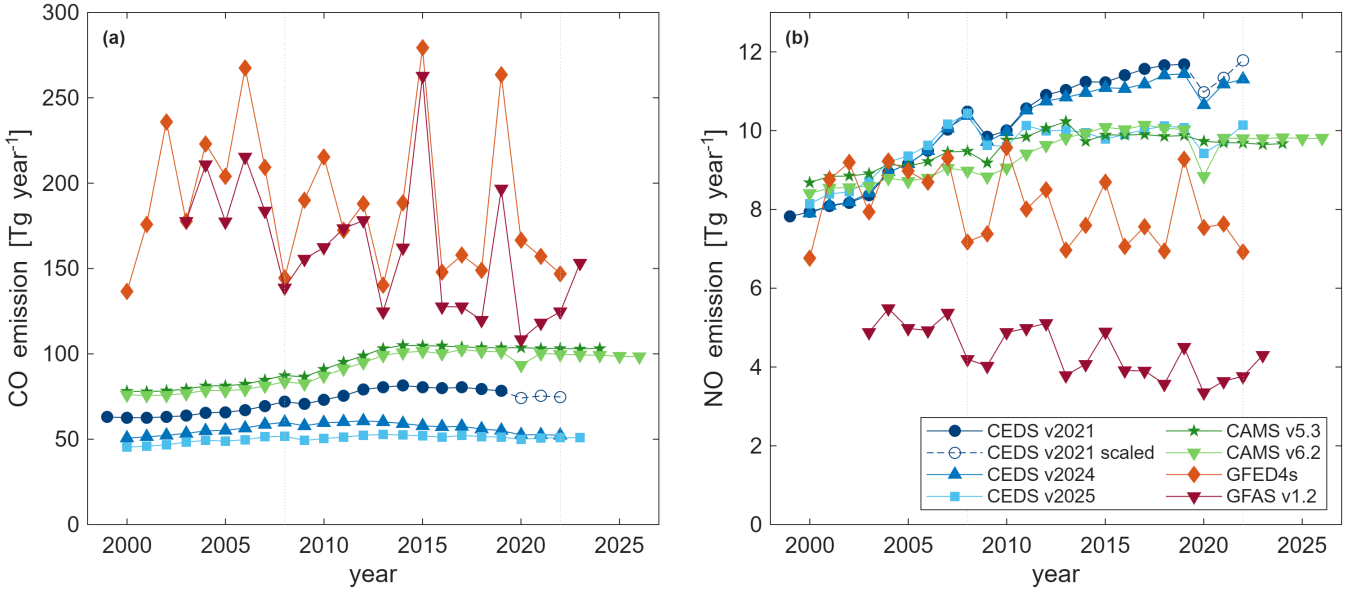

Figure 10. Changes of inventory anthropogenic (CEDS & CAMS) and biomass burning (GFED & GFAS) emissions between 2000 and 2026 of **(a)** carbon monoxide and **(b)** nitric oxide.

20 %), but are dominated by year-to-year variability. Emissions vary between 110-140 Tg CO for low fire years and up to 260-280 Tg for years with peak fire intensities. Overall emissions are 15-20 % higher in GFED compared to GFAS. Recent literature suggests that both inventories under-predict biomass burning CO emissions due to the incomplete detection of small fire sources (Mota and Wooster, 2018; van der Velde et al., 2024). Anthropogenic CO emissions estimates show large differences in magnitude and trend, both between different inventories and versions of the same inventory. CEDS v2021 (used to drive the GEOS-Chem simulations) suggests a gradual increase of CO emissions of around 30 % between 2000 and 2014 and a subtle decline of $<$10 % from 2014 onward. In contrast, CAMS CO emissions (green) are around 20–25 % higher than that and CEDS v2024 and v2025 suggest mostly constant CO emissions over time. Between 2014 and 2022, the latest CAMS and the latest CEDS versions differ by a factor of almost 2. This highlights a large uncertainty in the anthropogenic emission inventories employed in current models - particularly in the Southern Hemisphere. While Northern Hemispheric emission trends are not consistent across inventories either, the difference is generally within 20 %.

Figure 10(b) shows early 21st century trends in emission estimates of nitric oxide (NO), which indirectly affects CO by regulating the abundance of OH radicals via secondary production (Levy, 1971). Fire emissions of NO from the GFED4s emission inventory exhibit a subtle decline between 2000 and 2022 (p-value=0.07), but are dominated by year-to-year variability. GFAS v1.2 emissions are 40-50 % lower in line with findings by Marais et al. (2025). Anthropogenic NO emission estimates agree within 10–15 % between 2000 and 2010 with ∼20 % growth in emissions. While the CAMS and the CEDS v2025 NO emissions level off after 2010, CEDS v2021 and v2024 emission estimates increase by an additional ∼10 % in the following decade. The maximum annual difference between the inventories is around 20 %. Neither the overall SH NO

https://doi.org/10.5194/egusphere-2026-5476
Preprint. Discussion started: 11 September 2026

emissions nor the simulated NO mixing ratios (using GFED4s and CEDS v2021) in the southern extratropics show significant changes over time. In comparison, OMI NO_2 columns show significant upward trends in the southern extratropics (Figure S13). However, the retrieved values are mostly below the detection limit of the satellite instrument.

Simulated OH radical concentrations show small decreases at the surface, but no changes in the free troposphere and the simulations do not show significant changes in the CO loss term over the past 15 years. Finally, the production of CO from CH_4 oxidation via Cl radicals is a negligible pathway in GEOS-Chem, and is therefore not impacted by changes in Cl concentrations. Due to the lifetime of CO of weeks to months, which is on the timescale of intra-hemispheric mixing, it is unlikely that altered transport processes within the Southern Hemisphere contribute to the observed enhancements. There is no evidence that large scale transport patterns such as the Hadley circulation or the Brewer-Dobson circulation have changed to a degree, which could explain the CO increase over the past two decades, (Diallo et al., 2021; Kim et al., 2022). Small net increases of the downward flux from the stratosphere to the troposphere as reported by Škerlak et al. (2014) (for 2000–2011) would have the opposite effect (from that simulated) on CO levels.

Uncertainties in the model can result from the choice of emission inventories or the representation of tropospheric oxidants. Current anthropogenic emission estimates for CO vary by up to a factor of 2 among inventories in the Southern Hemisphere, biomass burning inventories for CO likely underestimate the actual emissions, and emissions of related species, such as biogenic NMVOCs from MEGAN are also not well constrained.

Wang et al. (2021) show that the Cl-containing species BrCl, Cl_2 and $ClNO_2$ observed during the ATom-3 and ATom-4 deployments are strongly underestimated in GEOS-Chem. It is therefore probable that methane oxidation by Cl is underestimated in the model. However, this underestimate is unlikely to be sufficient to contribute to the CO trend.

Changes in OH radicals over the past 15 years could be under-represented. Some recent modeling studies suggest that OH increased by $\sim$0.1–0.3 % year^{-1} over the past decades (Naik et al., 2013; Stevenson et al., 2020; Morgenstern et al., 2025); this trend is not represented in GEOS-Chem. Other studies including Lelieveld et al. (2016), Nicely et al. (2018) and Murray et al. (2021) suggest stable or highly uncertain levels and even decreases of tropospheric OH over the same time period (Turner et al., 2017). A GEOS-Chem sensitivity study with a 4 % reduction in the tropospheric mass-weighted mean OH concentration (5.7 % decrease in the tropospheric OH burden in the SH) for 2018 results in a $\sim$3 % increase in CO at the investigated stations. If we assume that OH follows an increasing trend of 0.26 % year^{-1} based on Stevenson et al. (2020) and assume a linear relationship between the change in OH and the response in CO as inferred from the GEOS-Chem sensitivity study (OH_{all}), the resulting model trend in surface CO at sites in the extratropics is around 30 % lower and insignificant. This confirms that a plausible positive trend in OH could counteract some of the recent simulated CO increases via CH_4, biogenic NMVOCs and temperature.

However, while a weakening of the CO trend would increase the agreement with some observations (NOAA flasks, IASI, and MOPITT), it would simultaneously lead to discrepancies with other observations (CSIRO flasks, HIPPO and ATom).

https://doi.org/10.5194/egusphere-2026-5476
Preprint. Discussion started: 11 September 2026

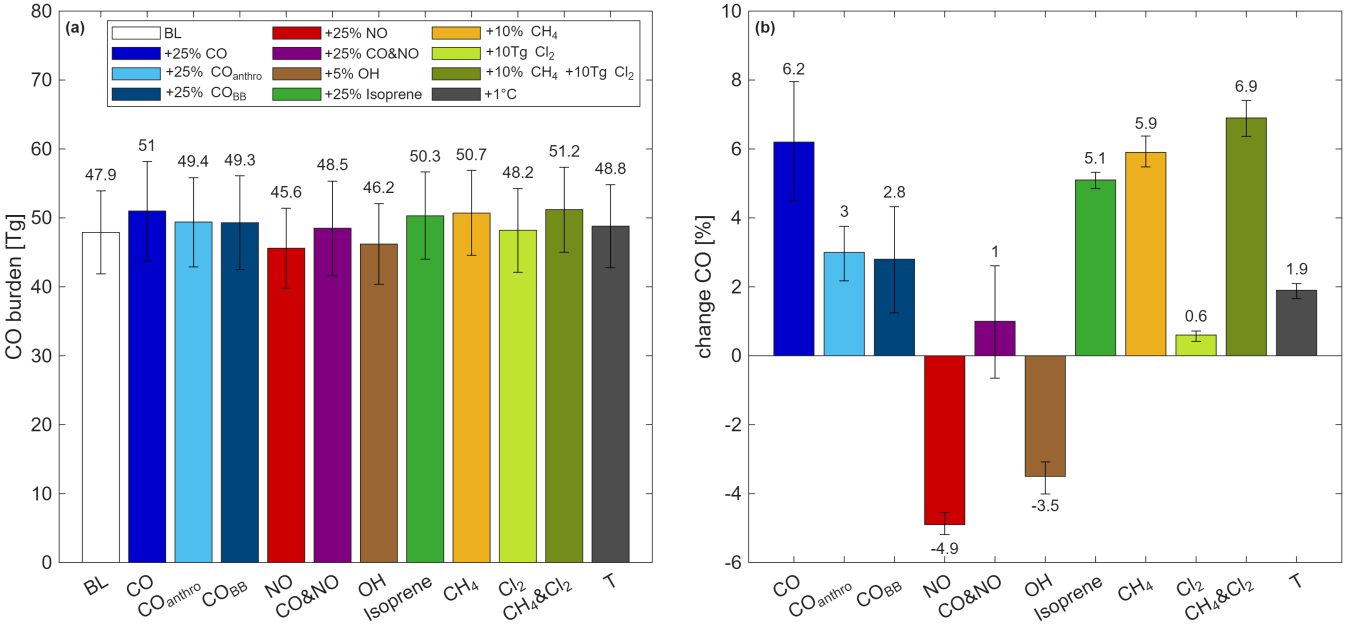

Figure 11. Summary of GEOS-Chem one-year sensitivity runs (2018). **(a)** Tropospheric burden (in Tg) of CO in the southern extratropics under the scenarios described in Table 1 (absolute numbers in Tg shown above the bars). **(b)** The resulting change in the CO burden relative to the baseline run (exact values above the bars). The error bars represent the 1σ variability throughout the year.

3.3 Future impacts on CO

In a changing climate and with an evolving emissions landscape, both the drivers responsible for recent trends and the excluded factors may affect tropospheric carbon monoxide in the remote Southern Hemisphere. To understand the impact of potential changes of these variables on CO in the future, we performed multiple GEOS-Chem sensitivity simulations (Table 1). Figure 11(a) provides an overview of the resulting CO burden in Tg in the southern extratropics. The baseline (BL) burden is 48 Tg (white bar). Figure 11(b) shows the relative change of the CO burden in each sensitivity run compared to the baseline.

CH_4 and biogenic NMVOC emission increases have contributed to CO enhancements since 2008 (Section 3.2). In a warming climate, these emissions are likely to increase further (e.g., Yvon-Durocher et al., 2014; Dean et al., 2018; Boy et al., 2022). A GEOS-Chem sensitivity study with a 10 % increase in surface CH_4 results in a ∼6 % increase in the CO burden ($CH_{4\ \mathrm{surface}}$). A 25 % increase in isoprene emissions ($\mathrm{Isoprene}_{\mathrm{all}}$) translates into a ∼5 % CO increase. If CH_4 and isoprene continue to increase at their current respective rates, these sensitivity scenarios will be reached in ∼20–30 years.

A comparable enhancement in CO levels would result from a 25 % increase in primary emissions ($\mathrm{CO}_{\mathrm{all}}$). Future CO emissions are highly uncertain. Under the SSP4-34 and SSP4-60 (Shared Socio-economic Pathways) scenarios, anthropogenic CO emissions from the Middle East and Africa region will increase ∼15 % by 2070 (and decline afterwards). The SSP3-baseline scenario predicts an emission increase for Latin America of 15 % by 2070 and 25 % by 2100. Under the SSP5-baseline scenario CO emissions from OECD countries, which also include Australia and New Zealand, will increase ∼10 % by 2080

https://doi.org/10.5194/egusphere-2026-5476
Preprint. Discussion started: 11 September 2026

(and decline afterwards) (Riahi et al., 2017). Climate change generally increases the potential for wildfires; however, other factors such as fire suppression or deforestation and changes in land use by humans can counter global trends in fire risk (Jones et al., 2022, 2024).

In contrast, increases in NO or OH would reduce CO. CO and NO are often co-emitted from primary sources and we therefore may experience similar changes in NO compared to CO in the future. A 25 % increase in NO emissions (NO_{all}) reduces CO by ∼5 % via accelerated OH recycling and enhanced CO loss. A simultaneous and uniform increase of CO and NO (CO_{all} & NO_{all}) leads to an overall modest increase of the CO burden (by ∼1 %). Potential increases in NO may enhance the availability of OH in the future. An isolated increase in the tropospheric mass-weighted mean OH concentration by 5 % (OH_{all}) reduces the CO burden in the southern extratropics by ∼3.5 %. Given the OH growth rates suggested in the current literature (∼0.05–0.3 % $year^{-1}$), this magnitude could be reached within the next three decades.

Similar to OH radicals, Cl radicals can oxidize CH_4. On a global scale, only a few percent (< 3 %) of CH_4 is lost via Cl, but the share can be higher locally (Hossaini et al., 2016; Sherwen et al., 2016; Wang et al., 2019). A large share of Cl originates from acid displacement of sea salt aerosol (Wang et al., 2021) and it has been reported that these emissions are increasing due to current increases in wind speeds over the Southern Ocean (Song et al., 2019; Zheng et al., 2022; Singer and Pincus, 2026) and the ongoing decline of Antarctic ice sheets (Yan et al., 2020). In a warming climate, this source of Cl could further increase. With an additional global 10 Tg Cl_2 ocean source ($Cl_{2\ ocean}$), the abundance of Cl radicals increases by ∼30 %, which leads to a 0.6 % increase in the CO burden in the SH extratropics. Simultaneous enhancements of Cl_2 and CH_4 ($Cl_{2\ ocean}$ & $CH_{4\ surface}$) lead to even larger CO increases relative to $Cl_{2\ ocean}$. Increases of Cl can therefore both enhance the CO burden directly and amplify the impact of CH_4 increases on CO through increased oxidation. However, the overall impact of Cl on CO is rather small and large changes would be needed to significantly impact the burden of CO.

Global temperatures are expected to rise in the coming years due to climate change; depending on the SSP scenario a 1 °C increase warming from current global mean temperatures could be reached between 2040 and 2060 (Gidden et al., 2019). Our sensitivity study suggests that the tropospheric CO burden in the southern extratropics would increase by 1.9 % in response to this 1 °C increase (T_{all}), and considerably more by the end of the century as warming accelerates.

4 Conclusions

In this study, we investigate changes in carbon monoxide in the remote Southern Hemisphere in recent decades in response to rapid increases in tropospheric CH_4 levels, as well as changes in other CO drivers, including primary emissions, precursor availability, and temperature. We explore these trends based on multi-platform observations from aircraft, surface, and satellite as well as global simulations with the chemistry-transport model GEOS-Chem.

We find that observed CO trends in the remote SH do not align across measurement programs. CSIRO surface flask observations of CO increase by ∼ 6–7 % between 2008 and 2022. In-situ high-frequency and PFP flask aircraft observations during ATom (2016–2018) show CO increases by ∼10 % compared to HIPPO (2009–2011). In contrast, CO observed from IASI shows smaller, insignificant upward trends. NOAA surface flask observations and MOPITT retrievals suggest constant

https://doi.org/10.5194/egusphere-2026-5476
Preprint. Discussion started: 11 September 2026

CO levels or even small, insignificant declines. Simulated remote SH carbon monoxide in the GEOS-Chem model increases by 6–7 % between 2008 and 2022, consistent with the trend in the airborne observations, the CSIRO surface flasks and the AGAGE in-situ measurements. While these enhancements are related to increased production from rising CH_4 levels and confirm our initial hypothesis, CH_4 enhancements account for only half of the overall simulated CO increase. Enhanced emissions of biogenic NMVOCs as well as increases in temperature, which accelerate the reaction rate of CH_4 with OH, contribute an additional 45 % and 5 %, respectively, to the trend. Potential reasons for the discrepancies among observations include measurement uncertainties, which arise in part from unique conditions in the Southern Hemisphere, including low concentrations, the long-term stability of CO calibration standards and the inter-comparability of different calibration scales.

Given a warming climate and a changing emissions landscape, many drivers may impact CO levels in the remote Southern Hemisphere in the coming decades. Potential future changes, which enhance CO levels, include increasing primary emissions from biomass burning and anthropogenic pollution, enhanced biogenic NMVOC emissions, increasing CH_4 from wetlands, enhanced availability of Cl radicals, as well as rising temperatures. In turn, potential increases of NO_x and OH could lead to CO reductions.

These results highlight the continuous need for the 4-dimensional monitoring of the atmospheric state and particularly for greater observational capacity in the Southern Hemisphere. Measurements in this hemisphere are still relatively sparse, but urgently needed considering current knowledge gaps in remote, Southern Hemispheric atmospheric composition. Carbon monoxide is involved in key processes affecting tropospheric levels of CH_4 and the oxidizing capacity, and is therefore a valuable indicator of how the atmospheric composition in remote locations is changing in response to anthropogenic perturbations. A continued effort to improve CO calibration scales, which most current measurement techniques rely on, will enhance the accuracy of CO measurements and, therefore, our understanding of its drivers in the troposphere. This study emphasizes the interplay of numerous processes in controlling reactive trace gas levels in the remote Southern Hemisphere. In the future, more research focusing on the sensitivity of these processes to alterations in the emission landscape and a changing climate is needed, with the goal of understanding and monitoring the implications for the atmospheric oxidizing capacity and the lifetime of greenhouse gases.

Data availability. The in-situ high frequency HIPPO and ATom datasets are available from Wofsy et al. (2017) and Wofsy et al. (2021), respectively. CO observations from the Programmable Flask Package (PFP) during HIPPO and ATom are provided by McKain et al. (2026). MOPITT data are available from NASA/LARC/SD/ASDC. Data from the IASI instrument are provided by Clerbaux and Coheur (2014). The NOAA Cooperative Global Air Sampling Network flask CO measurements are available from Pétron et al. (2026). CSIRO flask data are available from the World Data Center for Greenhouse Gases (WDCGG) (2025). Continuous AGAGE CO measurements are obtained from Prinn et al. (2025). The supporting data for this study will be available from zenodo: https://doi.org/10.5281/zenodo.20538812 after publication of this manuscript (Nussbaumer and Heald, 2026).

https://doi.org/10.5194/egusphere-2026-5476
Preprint. Discussion started: 11 September 2026

Author contributions. CMN and CLH conceptualized the study and interpreted the data. CMN performed the simulations, carried out the analysis and prepared the figures. TC, EAK, KM and SCW measured and provided the aircraft CO data. PBK, RLL, MM, KM and GP measured and provided the CO flask data. AGAGE CO data was obtained from AS. All co-authors contributed to reviewing and proofreading of the manuscript.

Competing interests. At least one of the (co-)authors is a member of the editorial board of Atmospheric Chemistry and Physics.

Acknowledgements. We thank Gonzalo González Abad for valuable discussions and advice on the analysis of OMI HCHO data. We further acknowledge Andrew Crotwell for his important work on the CO calibration scale revision (CO X2025).

https://doi.org/10.5194/egusphere-2026-5476
Preprint. Discussion started: 11 September 2026

References

Astoreca, R., Coheur, P., Hurtmans, D., Hadji-Lazaro, J., and George, M.: Product User Manual: Near real-time IASI CO, Tech. Rep. SAF/O3M/ULB/PUM/001, Université Libre de Bruxelles and LATMOS, https://satellites.aeronomie.be/index.php/support/documentation, 2016.

Bates, K. H., Evans, M. J., Henderson, B. H., and Jacob, D. J.: Impacts of updated reaction kinetics on the global GEOS-Chem simulation of atmospheric chemistry, Geoscientific Model Development, 17, 1511–1524, https://doi.org/10.5194/gmd-17-1511-2024, 2024.

Bey, I., Jacob, D. J., Yantosca, R. M., Logan, J. A., Field, B. D., Fiore, A. M., Li, Q., Liu, H. Y., Mickley, L. J., and Schultz, M. G.: Global modeling of tropospheric chemistry with assimilated meteorology: Model description and evaluation, Journal of Geophysical Research: Atmospheres, 106, 23 073–23 095, https://doi.org/10.1029/2001JD000807, 2001.

Bourgeois, I., Peischl, J., Thompson, C. R., Aikin, K. C., Campos, T., Clark, H., Commane, R., Daube, B., Diskin, G. W., Elkins, J. W., Gao, R.-S., Gaudel, A., Hintsa, E. J., Johnson, B. J., Kivi, R., McKain, K., Moore, F. L., Parrish, D. D., Querel, R., Ray, E., Sánchez, R., Sweeney, C., Tarasick, D. W., Thompson, A. M., Thouret, V., Witte, J. C., Wofsy, S. C., and Ryerson, T. B.: Global-scale distribution of ozone in the remote troposphere from the ATom and HIPPO airborne field missions, Atmospheric Chemistry and Physics, 20, 10 611–10 635, https://doi.org/10.5194/acp-20-10611-2020, 2020.

Bourgeois, I., Peischl, J., Neuman, J. A., Brown, S. S., Thompson, C. R., Aikin, K. C., Allen, H. M., Angot, H., Apel, E. C., Baublitz, C. B., Brewer, J. F., Campuzano-Jost, P., Commane, R., Crounse, J. D., Daube, B. C., DiGangi, J. P., Diskin, G. S., Emmons, L. K., Fiore, A. M., Gkatzelis, G. I., Hills, A., Hornbrook, R. S., Huey, L. G., Jimenez, J. L., Kim, M., Lacey, F., McKain, K., Murray, L. T., Nault, B. A., Parrish, D. D., Ray, E., Sweeney, C., Tanner, D., Wofsy, S. C., and Ryerson, T. B.: Large contribution of biomass burning emissions to ozone throughout the global remote troposphere, Proceedings of the National Academy of Sciences, 118, e2109628 118, https://doi.org/10.1073/pnas.2109628118, 2021.

Bowman, K. P.: Transport of carbon monoxide from the tropics to the extratropics, Journal of Geophysical Research: Atmospheres, 111, https://doi.org/10.1029/2005JD006137, 2006.

Boy, M., Zhou, P., Kurtén, T., Chen, D., Xavier, C., Clusius, P., Roldin, P., Baykara, M., Pichelstorfer, L., Foreback, B., Bäck, J., Petäjä, T., Makkonen, R., Kerminen, V.-M., Pihlatie, M., Aalto, J., and Kulmala, M.: Positive feedback mechanism between biogenic volatile organic compounds and the methane lifetime in future climates, npj Climate and Atmospheric Science, 5, 72, https://doi.org/10.1038/s41612-022-00292-0, 2022.

Buchholz, R. R., Worden, H. M., Park, M., Francis, G., Deeter, M. N., Edwards, D. P., Emmons, L. K., Gaubert, B., Gille, J., Martínez-Alonso, S., Tang, W., Kumar, R., Drummond, J. R., Clerbaux, C., George, M., Coheur, P.-F., Hurtmans, D., Bowman, K. W., Luo, M., Payne, V. H., Worden, J. R., Chin, M., Levy, R. C., Warner, J., Wei, Z., and Kulawik, S. S.: Air pollution trends measured from Terra: CO and AOD over industrial, fire-prone, and background regions, Remote Sensing of Environment, 256, 112 275, https://doi.org/10.1016/j.rse.2020.112275, 2021.

Carlier, P., Hannachi, H., and Mouvier, G.: The chemistry of carbonyl compounds in the atmosphere—A review, Atmospheric Environment (1967), 20, 2079–2099, https://doi.org/10.1016/0004-6981(86)90304-5, 1986.

Chen, Y., Hall, J., van Wees, D., Andela, N., Hantson, S., Giglio, L., van der Werf, G. R., Morton, D. C., and Randerson, J. T.: Multi-decadal trends and variability in burned area from the fifth version of the Global Fire Emissions Database (GFED5), Earth System Science Data, 15, 5227–5259, https://doi.org/10.5194/essd-15-5227-2023, 2023.

https://doi.org/10.5194/egusphere-2026-5476
Preprint. Discussion started: 11 September 2026

Clerbaux, C. and Coheur, P.-F.: Monthly IASI/Metop-B ULB-LATMOS carbon monoxide (CO) L3 product (total column), [dataset], https://doi.org/10.25326/748, 2014.

Clerbaux, C., Boynard, A., Clarisse, L., George, M., Hadji-Lazaro, J., Herbin, H., Hurtmans, D., Pommier, M., Razavi, A., Turquety, S., Wespes, C., and Coheur, P.-F.: Monitoring of atmospheric composition using the thermal infrared IASI/MetOp sounder, Atmospheric Chemistry and Physics, 9, 6041–6054, https://doi.org/10.5194/acp-9-6041-2009, 2009.

Conte, L., Szopa, S., Séférian, R., and Bopp, L.: The oceanic cycle of carbon monoxide and its emissions to the atmosphere, Biogeosciences, 16, 881–902, https://doi.org/10.5194/bg-16-881-2019, 2019.

Copernicus Atmosphere Monitoring Service: CAMS global biomass burning emissions based on fire radiative power (GFAS), Copernicus Atmosphere Monitoring Service (CAMS) Atmosphere Data Store, https://doi.org/10.24381/a05253c7, accessed: 2026-03-16, 2022.

Copernicus Atmosphere Monitoring Service: CAMS-GLOB-ANT v5.3, https://eccad.aeris-data.fr/, accessed: 2026-03-16, 2024.

Copernicus Atmosphere Monitoring Service: CAMS-GLOB-ANT v6.2, https://eccad.aeris-data.fr/, accessed: 2026-03-16, 2026.

Crutzen, P. J., Heidt, L. E., Krasnec, J. P., Pollock, W. H., and Seiler, W.: Biomass burning as a source of atmospheric gases CO, H2, N2O, NO, CH3Cl and COS, Nature, 282, 253–256, https://doi.org/10.1038/282253a0, 1979.

CSIRO: GASLab/AGGON, https://research.csiro.au/acc/capabilities/gaslab/, accessed: 2026-07-15, 2021.

Dean, J. F., Middelburg, J. J., Röckmann, T., Aerts, R., Blauw, L. G., Egger, M., Jetten, M. S. M., de Jong, A. E. E., Meisel, O. H., Rasigraf, O., Slomp, C. P., in't Zandt, M. H., and Dolman, A. J.: Methane Feedbacks to the Global Climate System in a Warmer World, Reviews of Geophysics, 56, 207–250, https://doi.org/https://doi.org/10.1002/2017RG000559, 2018.

Deeter, M., Francis, G., Gille, J., Mao, D., Martínez-Alonso, S., Worden, H., Ziskin, D., Drummond, J., Commane, R., Diskin, G., and McKain, K.: The MOPITT Version 9 CO product: sampling enhancements and validation, Atmospheric Measurement Techniques, 15, 2325–2344, https://doi.org/10.5194/amt-15-2325-2022, 2022.

Diallo, M., Ern, M., and Ploeger, F.: The advective Brewer–Dobson circulation in the ERA5 reanalysis: climatology, variability, and trends, Atmospheric Chemistry and Physics, 21, 7515–7544, https://doi.org/10.5194/acp-21-7515-2021, 2021.

Faïn, X., Rhodes, R. H., Place, P., Petrenko, V. V., Fourteau, K., Chellman, N., Crosier, E., McConnell, J. R., Brook, E. J., Blunier, T., Legrand, M., and Chappellaz, J.: Northern Hemisphere atmospheric history of carbon monoxide since preindustrial times reconstructed from multiple Greenland ice cores, Climate of the Past, 18, 631–647, https://doi.org/10.5194/cp-18-631-2022, 2022.

Faïn, X., Etheridge, D. M., Fourteau, K., Martinerie, P., Trudinger, C. M., Rhodes, R. H., Chellman, N. J., Langenfelds, R. L., McConnell, J. R., Curran, M. A. J., Brook, E. J., Blunier, T., Teste, G., Grilli, R., Lemoine, A., Sturges, W. T., Vannière, B., Freitag, J., and Chappellaz, J.: Southern Hemisphere atmospheric history of carbon monoxide over the late Holocene reconstructed from multiple Antarctic ice archives, Climate of the Past, 19, 2287–2311, https://doi.org/10.5194/cp-19-2287-2023, 2023.

Fortems-Cheiney, A., Chevallier, F., Pison, I., Bousquet, P., Saunois, M., Szopa, S., Cressot, C., Kurosu, T., Chance, K., and Fried, A.: The formaldehyde budget as seen by a global-scale multi-constraint and multi-species inversion system, Atmospheric Chemistry and Physics, 12, 6699–6721, https://doi.org/10.5194/acp-12-6699-2012, 2012.

Francey, R. J., Steele, L. P., Spencer, D. A., Langenfelds, R. L., Law, R. M., Krummel, P. B., Fraser, P. J., Etheridge, D. M., Derek, N., Coram, S. A., Cooper, L. N., Allison, C. E., Porter, L., and Baly, S.: The CSIRO (Australia) Measurement of Greenhouse Gases in the Global Atmosphere, in: Report of the 11th WMO/IAEA Meeting of Experts on Carbon Dioxide Concentration and Related Tracer Measurement Techniques, Tokyo, Japan, September 2001, edited by Toru, S. and Kazuto, S., 148, pp. 97–111, World Meteorological Organization Global Atmosphere Watch, 2003.

https://doi.org/10.5194/egusphere-2026-5476
Preprint. Discussion started: 11 September 2026

García, O. E., Sepúlveda, E., Schneider, M., Hase, F., August, T., Blumenstock, T., Kühl, S., Munro, R., Gómez-Peláez, A. J., Hultberg, T., Redondas, A., Barthlott, S., Wiegele, A., González, Y., and Sanromá, E.: Consistency and quality assessment of the Metop-A/IASI and Metop-B/IASI operational trace gas products (O_3, CO, N_2O, CH_4, and CO_2) in the subtropical North Atlantic, Atmospheric Measurement Techniques, 9, 2315–2333, https://doi.org/10.5194/amt-9-2315-2016, 2016.

George, M., Clerbaux, C., Bouarar, I., Coheur, P.-F., Deeter, M. N., Edwards, D. P., Francis, G., Gille, J. C., Hadji-Lazaro, J., Hurtmans, D., Inness, A., Mao, D., and Worden, H. M.: An examination of the long-term CO records from MOPITT and IASI: comparison of retrieval methodology, Atmospheric Measurement Techniques, 8, 4313–4328, https://doi.org/10.5194/amt-8-4313-2015, 2015.

GEOS-Chem: Overview, https://geoschem.github.io/overview.html, accessed: 2026-02-24, 2026.

Gidden, M. J., Riahi, K., Smith, S. J., Fujimori, S., Luderer, G., Kriegler, E., van Vuuren, D. P., van den Berg, M., Feng, L., Klein, D., Calvin, K., Doelman, J. C., Frank, S., Fricko, O., Harmsen, M., Hasegawa, T., Havlik, P., Hilaire, J., Hoesly, R., Horing, J., Popp, A., Stehfest, E., and Takahashi, K.: Global emissions pathways under different socioeconomic scenarios for use in CMIP6: a dataset of harmonized emissions trajectories through the end of the century, Geoscientific Model Development, 12, 1443–1475, https://doi.org/10.5194/gmd-12-1443-2019, 2019.

Gloudemans, A. M. S., Krol, M. C., Meirink, J. F., de Laat, A. T. J., van der Werf, G. R., Schrijver, H., van den Broek, M. M. P., and Aben, I.: Evidence for long-range transport of carbon monoxide in the Southern Hemisphere from SCIAMACHY observations, Geophysical Research Letters, 33, https://doi.org/10.1029/2006GL026804, 2006.

Gonzalez Abad, G. and Sun, K.: README Document for OMHCHOd, Tech. rep., NASA Goddard Earth Sciences Data and Information Services Center (GES DISC), Greenbelt, MD, USA, https://acdisc.gesdisc.eosdis.nasa.gov/data/Aura_OMI_Level3/OMHCHOd.003/doc/README_OMHCHOd_v003.pdf, reviewed by James E. Johnson (GES DISC, GSFC Code 610.2). Last revised August 20, 2019, 2019.

Griffin, D., Chen, J., Anderson, K., Makar, P., McLinden, C. A., Dammers, E., and Fogal, A.: Biomass burning CO emissions: exploring insights through TROPOMI-derived emissions and emission coefficients, Atmospheric Chemistry and Physics, 24, 10 159–10 186, https://doi.org/10.5194/acp-24-10159-2024, 2024.

Guenther, A., Karl, T., Harley, P., Wiedinmyer, C., Palmer, P. I., and Geron, C.: Estimates of global terrestrial isoprene emissions using MEGAN (Model of Emissions of Gases and Aerosols from Nature), Atmospheric Chemistry and Physics, 6, 3181–3210, https://doi.org/10.5194/acp-6-3181-2006, 2006.

Heald, C. L., Jacob, D. J., Fiore, A. M., Emmons, L. K., Gille, J. C., Deeter, M. N., Warner, J., Edwards, D. P., Crawford, J. H., Hamlin, A. J., Sachse, G. W., Browell, E. V., Avery, M. A., Vay, S. A., Westberg, D. J., Blake, D. R., Singh, H. B., Sandholm, S. T., Talbot, R. W., and Fuelberg, H. E.: Asian outflow and trans-Pacific transport of carbon monoxide and ozone pollution: An integrated satellite, aircraft, and model perspective, Journal of Geophysical Research: Atmospheres, 108, https://doi.org/https://doi.org/10.1029/2003JD003507, 2003.

Heald, C. L., Kroll, J. H., Murphy, J. G., Farmer, D. K., and Fry, J. L.: Atmospheric Chemistry Insights from the Global COVID-19 Pandemic: A Review, Environmental Science & Technology, 60, 10 393–10 404, https://doi.org/10.1021/acs.est.5c16737, 2026.

Hedelius, J. K., Toon, G. C., Buchholz, R. R., Iraci, L. T., Podolske, J. R., Roehl, C. M., Wennberg, P. O., Worden, H. M., and Wunch, D.: Regional and Urban Column CO Trends and Anomalies as Observed by MOPITT Over 16 Years, Journal of Geophysical Research: Atmospheres, 126, e2020JD033 967, https://doi.org/10.1029/2020JD033967, 2021.

Hoesly, R. M., Smith, S. J., Feng, L., Klimont, Z., Janssens-Maenhout, G., Pitkanen, T., Seibert, J. J., Vu, L., Andres, R. J., Bolt, R. M., Bond, T. C., Dawidowski, L., Kholod, N., Kurokawa, J.-I., Li, M., Liu, L., Lu, Z., Moura, M. C. P., O'Rourke, P. R., and Zhang, Q.: Historical

https://doi.org/10.5194/egusphere-2026-5476
Preprint. Discussion started: 11 September 2026

(1750–2014) anthropogenic emissions of reactive gases and aerosols from the Community Emissions Data System (CEDS), Geoscientific Model Development, 11, 369–408, https://doi.org/10.5194/gmd-11-369-2018, 2018.

Holloway, T., Levy II, H., and Kasibhatla, P.: Global distribution of carbon monoxide, Journal of Geophysical Research: Atmospheres, 105, 12 123–12 147, https://doi.org/10.1029/1999JD901173, 2000.

Hossaini, R., Chipperfield, M. P., Saiz-Lopez, A., Fernandez, R., Monks, S., Feng, W., Brauer, P., and von Glasow, R.: A global model of tropospheric chlorine chemistry: Organic versus inorganic sources and impact on methane oxidation, Journal of Geophysical Research: Atmospheres, 121, 14,271–14,297, https://doi.org/10.1002/2016JD025756, 2016.

Hudman, R. C., Moore, N. E., Mebust, A. K., Martin, R. V., Russell, A. R., Valin, L. C., and Cohen, R. C.: Steps towards a mechanistic model of global soil nitric oxide emissions: implementation and space based-constraints, Atmospheric Chemistry and Physics, 12, 7779–7795, https://doi.org/10.5194/acp-12-7779-2012, 2012.

Hurtmans, D., Coheur, P.-F., Wespes, C., Clarisse, L., Scharf, O., Clerbaux, C., Hadji-Lazaro, J., George, M., and Turquety, S.: FORLI radiative transfer and retrieval code for IASI, Journal of Quantitative Spectroscopy and Radiative Transfer, 113, 1391–1408, https://doi.org/10.1016/j.jqsrt.2012.02.036, 2012.

IPCC: Climate Change 2021: The Physical Science Basis. Contribution of Working Group I to the Sixth Assessment Report of the Intergovernmental Panel on Climate Change, Cambridge University Press, Cambridge, United Kingdom and New York, NY, USA, https://doi.org/10.1017/9781009157896, 2021.

Jaffe, D., Mahura, A., Kelley, J., Atkins, J., Novelli, P. C., and Merrill, J.: Impact of Asian emissions on the remote North Pacific atmosphere: Interpretation of CO data from Shemya, Guam, Midway and Mauna Loa, Journal of Geophysical Research: Atmospheres, 102, 28 627–28 635, https://doi.org/10.1029/96JD02750, 1997.

Jiang, Z., Worden, J. R., Worden, H., Deeter, M., Jones, D. B., Arellano, A. F., and Henze, D. K.: A 15-year record of CO emissions constrained by MOPITT CO observations, Atmospheric Chemistry and Physics, 17, 4565–4583, https://doi.org/10.5194/acp-17-4565-2017, 2017.

Jiang, Z., McDonald, B. C., Worden, H., Worden, J. R., Miyazaki, K., Qu, Z., Henze, D. K., Jones, D. B. A., Arellano, A. F., Fischer, E. V., Zhu, L., and Boersma, K. F.: Unexpected slowdown of US pollutant emission reduction in the past decade, Proceedings of the National Academy of Sciences, 115, 5099–5104, https://doi.org/10.1073/pnas.1801191115, 2018.

Johnson, M. S., Philip, S., Meech, S., Kumar, R., Sorek-Hamer, M., Shiga, Y. P., and Jung, J.: Insights into the long-term (2005–2021) spatiotemporal evolution of summer ozone production sensitivity in the Northern Hemisphere derived with the Ozone Monitoring Instrument (OMI), Atmospheric Chemistry and Physics, 24, 10 363–10 384, https://doi.org/10.5194/acp-24-10363-2024, 2024.

Joint Global Change Research Institute: CEDS, https://github.com/JGCRI/CEDS/tree/master, accessed: 2026-03-17, 2025a.

Joint Global Change Research Institute: CEDS v2024-11-25, https://metagrid.esgf-west.org/search/input4mips/, accessed: 2026-03-6, 2025b.

Joint Global Change Research Institute: CEDS v2025-04-18, https://metagrid.esgf-west.org/search/input4mips/, accessed: 2026-03-6, 2025c.

Jones, M. W., Abatzoglou, J. T., Veraverbeke, S., Andela, N., Lasslop, G., Forkel, M., Smith, A. J. P., Burton, C., Betts, R. A., van der Werf, G. R., Sitch, S., Canadell, J. G., Santín, C., Kolden, C., Doerr, S. H., and Le Quéré, C.: Global and Regional Trends and Drivers of Fire Under Climate Change, Reviews of Geophysics, 60, e2020RG000 726, https://doi.org/10.1029/2020RG000726, 2022.

Jones, M. W., Veraverbeke, S., Andela, N., Doerr, S. H., Kolden, C., Mataveli, G., Pettinari, M. L., Le Quéré, C., Rosan, T. M., van der Werf, G. R., van Wees, D., and Abatzoglou, J. T.: Global rise in forest fire emissions linked to climate change in the extratropics, Science, 386, eadl5889, https://doi.org/10.1126/science.adl5889, 2024.

https://doi.org/10.5194/egusphere-2026-5476
Preprint. Discussion started: 11 September 2026

Kaiser, J. W., Heil, A., Andreae, M. O., Benedetti, A., Chubarova, N., Jones, L., Morcrette, J.-J., Razinger, M., Schultz, M. G., Suttie, M., and van der Werf, G. R.: Biomass burning emissions estimated with a global fire assimilation system based on observed fire radiative power, Biogeosciences, 9, 527–554, https://doi.org/10.5194/bg-9-527-2012, 2012.

Keller, C. A., Long, M. S., Yantosca, R. M., Da Silva, A. M., Pawson, S., and Jacob, D. J.: HEMCO v1.0: a versatile, ESMF-compliant component for calculating emissions in atmospheric models, Geoscientific Model Development, 7, 1409–1417, https://doi.org/10.5194/gmd-7-1409-2014, 2014.

Khalil, M. and Rasmussen, R.: The global cycle of carbon monoxide: Trends and mass balance, Chemosphere, 20, 227–242, https://doi.org/10.1016/0045-6535(90)90098-E, 1990.

Kim, D., Kim, H., Kang, S. M., Stuecker, M. F., and Merlis, T. M.: Weak Hadley cell intensity changes due to compensating effects of tropical and extratropical radiative forcing, NPJ Climate and Atmospheric Science, 5, 61, https://doi.org/10.1038/s41612-022-00287-x, 2022.

Lan, X., T. P. T. K. . N.: NOAA Greenhouse Gas Marine Boundary Layer Reference - CH4, https://doi.org/https://doi.org/10.15138/DVNP-F961, [Dataset], 2024.

Lan, X., Petron, G., Baugh, K., Crotwell, A. M., Crotwell, M. J., DeVogel, S., Madronich, M., Mauss, J., Mefford, T., Moglia, E., Morris, S., Mund, J. W., Searle, A., Thoning, K. W., Wolter, S., and Miller, J.: Atmospheric Methane Dry Air Mole Fractions from the NOAA GML Global Greenhouse Gas Reference Network, Carbon Cycle Cooperative Global Air Sampling Network: 1983 - Present, NOAA Global Monitoring Laboratory, https://doi.org/10.15138/VNCZ-M766, version: 2025-04-26, 2025.

Lan, X., Thoning, K. W., and Dlugokencky, E. J.: Trends in globally-averaged CH4, N2O, and SF6 determined from NOAA Global Monitoring Laboratory measurements, NOAA Global Monitoring Laboratory, https://doi.org/10.15138/P8XG-AA10, accessed: 2026-07-15, 2026.

Langenfelds, R. L., Guérette, E.-A., Steele, L. P., Krummel, P. B., Spencer, D. A., Loh, Z. M., Gregory, R. L., Thornton, D. P., Howden, R. T., and Fraser, P. J.: Atmospheric Methane, Carbon Dioxide, Hydrogen, Carbon Monoxide and Nitrous Oxide from Cape Grim Flask Air Samples Analysed by Gas Chromatography, Tech. rep., Melbourne, Australia, in press, 2026.

Lee, M., Heikes, B. G., and Jacob, D. J.: Enhancements of hydroperoxides and formaldehyde in biomass burning impacted air and their effect on atmospheric oxidant cycles, Journal of Geophysical Research: Atmospheres, 103, 13 201–13 212, https://doi.org/10.1029/98JD00578, 1998.

Lelieveld, J., Gromov, S., Pozzer, A., and Taraborrelli, D.: Global tropospheric hydroxyl distribution, budget and reactivity, Atmospheric Chemistry and Physics, 16, 12 477–12 493, https://doi.org/10.5194/acp-16-12477-2016, 2016.

Levy, H.: Normal Atmosphere: Large Radical and Formaldehyde Concentrations Predicted, Science, 173, 141–143, https://doi.org/10.1126/science.173.3992.141, 1971.

Levy II, H.: Tropospheric budgets for methane, carbon monoxide, and related species, Journal of Geophysical Research (1896-1977), 78, 5325–5332, https://doi.org/10.1029/JC078i024p05325, 1973.

Lin, H., Jacob, D. J., Lundgren, E. W., Sulprizio, M. P., Keller, C. A., Fritz, T. M., Eastham, S. D., Emmons, L. K., Campbell, P. C., Baker, B., Saylor, R. D., and Montuoro, R.: Harmonized Emissions Component (HEMCO) 3.0 as a versatile emissions component for atmospheric models: application in the GEOS-Chem, NASA GEOS, WRF-GC, CESM2, NOAA GEFS-Aerosol, and NOAA UFS models, Geoscientific Model Development, 14, 5487–5506, https://doi.org/10.5194/gmd-14-5487-2021, 2021.

Logan, J. A., Prather, M. J., Wofsy, S. C., and McElroy, M. B.: Tropospheric chemistry: A global perspective, Journal of Geophysical Research: Oceans, 86, 7210–7254, https://doi.org/10.1029/JC086iC08p07210, 1981.

https://doi.org/10.5194/egusphere-2026-5476
Preprint. Discussion started: 11 September 2026

Marais, E. A., Van Damme, M., Clarisse, L., Wiedinmyer, C., Murphy, K., and van der Werf, G. R.: Subtropical southern Africa fire emissions of nitrogen oxides and ammonia obtained with satellite observations and GEOS-Chem, Environmental Science: Atmospheres, 5, 906–920, https://doi.org/10.1039/d5ea00041f, 2025.

McKain, K. and Sweeney, C.: ATom: CO2, CH4, and CO Measurements from Picarro, 2016-2018, https://doi.org/10.3334/ORNLDAAC/1732, accessed: 2026-08-12, 2021.

McKain, K., Sweeney, C., Baier, B., Baugh, K., Crotwell, A., Crotwell, M., Handley, P., Higgs, J., Kaiser, E., Madronich, M., Mauss, J. M., Miller, J. B., Moglia, E., Morris, S., Mund, J., Newberger, T., Petron, G., Verbeke, B., Wolter, S., and NOAA Global Monitoring Laboratory: NOAA Global Greenhouse Gas Reference Network Flask-Air PFP Sample Measurements of CO2, CH4, CO, N2O, H2, SF6 and isotopic ratios collected from aircraft vertical profiles, https://doi.org/10.15138/39HR-9N34, 2026.

MOPITT Algorithm Development Team: MOPITT (Measurements of Pollution in the Troposphere) Version 9 Product User's Guide, Tech. rep., Atmospheric Chemistry Observations and Modeling Laboratory, National Center for Atmospheric Research, Boulder, CO, https://www2.acom.ucar.edu/sites/default/files/documents/v9_users_guide_20220203.pdf, 2022.

Morgenstern, O., Moss, R., Manning, M., Zeng, G., Schaefer, H., Usoskin, I., Turnbull, J., Brailsford, G., Nichol, S., and Bromley, T.: Radiocarbon monoxide indicates increasing atmospheric oxidizing capacity, Nature Communications, 16, 249, https://doi.org/10.1038/s41467-024-55603-1, 2025.

Mota, B. and Wooster, M. J.: A new top-down approach for directly estimating biomass burning emissions and fuel consumption rates and totals from geostationary satellite fire radiative power (FRP), Remote Sensing of Environment, 206, 45–62, https://doi.org/10.1016/j.rse.2017.12.016, 2018.

Murray, L. T., Jacob, D. J., Logan, J. A., Hudman, R. C., and Koshak, W. J.: Optimized regional and interannual variability of lightning in a global chemical transport model constrained by LIS/OTD satellite data, Journal of Geophysical Research: Atmospheres, 117, https://doi.org/10.1029/2012JD017934, 2012.

Murray, L. T., Fiore, A. M., Shindell, D. T., Naik, V., and Horowitz, L. W.: Large uncertainties in global hydroxyl projections tied to fate of reactive nitrogen and carbon, Proceedings of the National Academy of Sciences, 118, e2115204118, https://doi.org/10.1073/pnas.2115204118, 2021.

Naik, V., Voulgarakis, A., Fiore, A. M., Horowitz, L. W., Lamarque, J.-F., Lin, M., Prather, M. J., Young, P. J., Bergmann, D., Cameron-Smith, P. J., Cionni, I., Collins, W. J., Dalsøren, S. B., Doherty, R., Eyring, V., Faluvegi, G., Folberth, G. A., Josse, B., Lee, Y. H., MacKenzie, I. A., Nagashima, T., van Noije, T. P. C., Plummer, D. A., Righi, M., Rumbold, S. T., Skeie, R., Shindell, D. T., Stevenson, D. S., Strode, S., Sudo, K., Szopa, S., and Zeng, G.: Preindustrial to present-day changes in tropospheric hydroxyl radical and methane lifetime from the Atmospheric Chemistry and Climate Model Intercomparison Project (ACCMIP), Atmospheric Chemistry and Physics, 13, 5277–5298, https://doi.org/10.5194/acp-13-5277-2013, 2013.

NASA/LARC/SD/ASDC: MOPITT Beta CO gridded monthly means (Near and Thermal Infrared Radiances) V009, https://doi.org/10.5067/TERRA/MOPITT/MOP03JM_L3.009.

Nicely, J. M., Canty, T. P., Manyin, M., Oman, L. D., Salawitch, R. J., Steenrod, S. D., Strahan, S. E., and Strode, S. A.: Changes in Global Tropospheric OH Expected as a Result of Climate Change Over the Last Several Decades, Journal of Geophysical Research: Atmospheres, 123, 10,774–10,795, https://doi.org/10.1029/2018JD028388, 2018.

NOAA: Cooperative Air Sampling Network, https://gml.noaa.gov/ccgg/flask.html, accessed: 2026-07-15, 2025.

NOAA Global Monitoring Laboratory: Carbon Monoxide (CO) WMO Scale: Scale update: WMO CO_X2025, https://gml.noaa.gov/ccl/co_scale.html, accessed: 2026-05-19, 2026.

https://doi.org/10.5194/egusphere-2026-5476
Preprint. Discussion started: 11 September 2026

NOAA GML: About the GGGRN, https://gml.noaa.gov/ccgg/about.html, accessed: 2026-07-29, 2025a.

NOAA GML: Curve Fitting Methods Applied to Time Series in NOAA GML, https://gml.noaa.gov/ccgg/mbl/crvfit/crvfit.html, acessed: 2026-07-21, 2025b.

Novelli, P. C., Masarie, K. A., Tans, P. P., and Lang, P. M.: Recent Changes in Atmospheric Carbon Monoxide, Science, 263, 1587–1590, https://doi.org/10.1126/science.263.5153.1587, 1994.

Novelli, P. C., Masarie, K. A., and Lang, P. M.: Distributions and recent changes of carbon monoxide in the lower troposphere, Journal of Geophysical Research: Atmospheres, 103, 19 015–19 033, https://doi.org/https://doi.org/10.1029/98JD01366, 1998.

Nussbaumer, C. M. and Heald, C. L.: Supporting data for: What controls tropospheric carbon monoxide in the remote Southern Hemisphere?, https://doi.org/10.5281/zenodo.20538812, 2026.

Okpalaonwuka, C., Udo, S., and Ewona, I.: Spatiotemporal variation and trend in carbon monoxide concentration over Africa: insights from MOPITT Data, Air Quality, Atmosphere & Health, 17, 469–484, https://doi.org/10.1007/s11869-023-01457-3, 2024.

OMI Nitrogen Dioxide Algorithm Team: OMNO2 README Document: Data Product Version 4.0, Tech. Rep. Document Version 9.0, NASA Goddard Space Flight Center, Greenbelt, MD, USA, https://aura.gesdisc.eosdis.nasa.gov/data/Aura_OMI_Level2/OMNO2.003/doc/README.OMNO2.pdf, team members: N. A. Krotkov, L. N. Lamsal, S. V. Marchenko, and W. H. Swartz. Covers products OMNO2, OMNO2G, and OMNO2D, 2019.

Patel, A., Mallik, C., Chandra, N., Patra, P. K., and Steinbacher, M.: Revisiting regional and seasonal variations in decadal carbon monoxide variability: Global reversal of growth rate, Science of The Total Environment, 909, 168 476, https://doi.org/10.1016/j.scitotenv.2023.168476, 2024.

Paton-Walsh, C., Emmerson, K. M., Garland, R. M., Keywood, M., Hoelzemann, J. J., Huneeus, N., Buchholz, R. R., Humphries, R. S., Altieri, K., Schmale, J., Wilson, S. R., Labuschagne, C., Kalisa, E., Fisher, J. A., Deutscher, N. M., van Zyl, P. G., Beukes, J. P., Joubert, W., Martin, L., Mkololo, T., Barbosa, C., de Fatima Andrade, M., Schofield, R., Mallet, M. D., Harvey, M. J., Formenti, P., Piketh, S. J., and Olivares, G.: Key challenges for tropospheric chemistry in the Southern Hemisphere, Elementa: Science of the Anthropocene, 10, 00 050, https://doi.org/10.1525/elementa.2021.00050, 2022.

Pétron, G., Lan, X., Baugh, K., Crotwell, A., Crotwell, M., DeVogel, S., Madronich, M., Mauss, J., Mefford, T., Moglia, E., Morris, S., Mund, J., Searle, A., Thoning, K., and J, M.: Atmospheric Carbon Monoxide Dry Air Mole Fractions from the NOAA GML Global Greenhouse Gas Reference Network, Carbon Cycle Cooperative Global Air Sampling Network: 1988 - Present, NOAA Global Monitoring Laboratory, https://doi.org/10.15138/33bv-s284, version: 2026-08-11, 2026.

Platt, U., Allan, W., and Lowe, D.: Hemispheric average Cl atom concentration from $^{13}C/^{12}C$ ratios in atmospheric methane, Atmospheric Chemistry and Physics, 4, 2393–2399, https://doi.org/10.5194/acp-4-2393-2004, 2004.

Poisson, N., Kanakidou, M., and Crutzen, P. J.: Impact of non-methane hydrocarbons on tropospheric chemistry and the oxidizing power of the global troposphere: 3-dimensional modelling results, Journal of Atmospheric Chemistry, 36, 157–230, https://doi.org/10.1023/A:1006300616544, 2000.

Pope, R. J., Kerridge, B. J., Siddans, R., Latter, B. G., Chipperfield, M. P., Arnold, S. R., Ventress, L. J., Pimlott, M. A., Graham, A. M., Knappett, D. S., and Rigby, R.: Large Enhancements in Southern Hemisphere Satellite-Observed Trace Gases Due to the 2019/2020 Australian Wildfires, Journal of Geophysical Research: Atmospheres, 126, e2021JD034 892, https://doi.org/https://doi.org/10.1029/2021JD034892, 2021.

Prather, M. J.: Photolysis rates in correlated overlapping cloud fields: Cloud-J 7.3c, Geoscientific Model Development, 8, 2587–2595, https://doi.org/10.5194/gmd-8-2587-2015, 2015.

https://doi.org/10.5194/egusphere-2026-5476
Preprint. Discussion started: 11 September 2026

Prinn, R., Weiss, R., Arduini, J., Choi, H., Engel, A., Fraser, P., Ganesan, A., Harth, C., Hermansen, O., Kim, J., Krummel, P., Loh, Z., Lunder, C., Maione, M., Manning, A., Mitrevski, B., Mühle, J., O'Doherty, S., Park, S., Pitt, J., Reimann, S., Rigby, M., Saito, T., Salameh, P., Schmidt, R., Simmonds, P., Stanley, K., Stavert, A., Steele, P., Vollmer, M., Wagenhäuser, T., Wang, H. J. R., Wenger, A., Western, L., Yao, B., Young, D., Zhou, L., and Zhu, L.: The dataset of in-situ measurements of chemically and radiatively important atmospheric gases from the Advanced Global Atmospheric Gas Experiment (AGAGE) and affiliated stations, https://doi.org/10.60718/2zet-cn22, 2025.

Prinn, R. G., Weiss, R. F., Arduini, J., Arnold, T., DeWitt, H. L., Fraser, P. J., Ganesan, A. L., Gasore, J., Harth, C. M., Hermansen, O., Kim, J., Krummel, P. B., Li, S., Loh, Z. M., Lunder, C. R., Maione, M., Manning, A. J., Miller, B. R., Mitrevski, B., Mühle, J., O'Doherty, S., Park, S., Reimann, S., Rigby, M., Saito, T., Salameh, P. K., Schmidt, R., Simmonds, P. G., Steele, L. P., Vollmer, M. K., Wang, R. H., Yao, B., Yokouchi, Y., Young, D., and Zhou, L.: History of chemically and radiatively important atmospheric gases from the Advanced Global Atmospheric Gases Experiment (AGAGE), Earth System Science Data, 10, 985–1018, https://doi.org/10.5194/essd-10-985-2018, 2018.

Riahi, K., van Vuuren, D. P., Kriegler, E., Edmonds, J., O'Neill, B. C., Fujimori, S., Bauer, N., Calvin, K., Dellink, R., Fricko, O., Lutz, W., Popp, A., Cuaresma, J. C., KC, S., Leimbach, M., Jiang, L., Kram, T., Rao, S., Emmerling, J., Ebi, K., Hasegawa, T., Havlik, P., Humpenöder, F., Da Silva, L. A., Smith, S., Stehfest, E., Bosetti, V., Eom, J., Gernaat, D., Masui, T., Rogelj, J., Strefler, J., Drouet, L., Krey, V., Luderer, G., Harmsen, M., Takahashi, K., Baumstark, L., Doelman, J. C., Kainuma, M., Klimont, Z., Marangoni, G., Lotze-Campen, H., Obersteiner, M., Tabeau, A., and Tavoni, M.: The Shared Socioeconomic Pathways and their energy, land use, and greenhouse gas emissions implications: An overview, Global Environmental Change, 42, 153–168, https://doi.org/10.1016/j.gloenvcha.2016.05.009, 2017.

Rigby, M., Montzka, S. A., Prinn, R. G., White, J. W. C., Young, D., O'Doherty, S., Lunt, M. F., Ganesan, A. L., Manning, A. J., Simmonds, P. G., Salameh, P. K., Harth, C. M., Mühle, J., Weiss, R. F., Fraser, P. J., Steele, L. P., Krummel, P. B., McCulloch, A., and Park, S.: Role of atmospheric oxidation in recent methane growth, Proceedings of the National Academy of Sciences, 114, 5373–5377, https://doi.org/10.1073/pnas.1616426114, 2017.

Santoni, G. W., Daube, B. C., Kort, E. A., Jiménez, R., Park, S., Pittman, J. V., Gottlieb, E., Xiang, B., Zahniser, M. S., Nelson, D. D., McManus, J. B., Peischl, J., Ryerson, T. B., Holloway, J. S., Andrews, A. E., Sweeney, C., Hall, B., Hintsa, E. J., Moore, F. L., Elkins, J. W., Hurst, D. F., Stephens, B. B., Bent, J., and Wofsy, S. C.: Evaluation of the airborne quantum cascade laser spectrometer (QCLS) measurements of the carbon and greenhouse gas suite ndash; CO_2, CH_4, N_2O, and CO ndash; during the CalNex and HIPPO campaigns, Atmospheric Measurement Techniques, 7, 1509–1526, https://doi.org/10.5194/amt-7-1509-2014, 2014.

Saunois, M., Stavert, A. R., Poulter, B., Bousquet, P., Canadell, J. G., Jackson, R. B., Raymond, P. A., Dlugokencky, E. J., Houweling, S., Patra, P. K., Ciais, P., Arora, V. K., Bastviken, D., Bergamaschi, P., Blake, D. R., Brailsford, G., Bruhwiler, L., Carlson, K. M., Carrol, M., Castaldi, S., Chandra, N., Crevoisier, C., Crill, P. M., Covey, K., Curry, C. L., Etiope, G., Frankenberg, C., Gedney, N., Hegglin, M. I., Höglund-Isaksson, L., Hugelius, G., Ishizawa, M., Ito, A., Janssens-Maenhout, G., Jensen, K. M., Joos, F., Kleinen, T., Krummel, P. B., Langenfelds, R. L., Laruelle, G. G., Liu, L., Machida, T., Maksyutov, S., McDonald, K. C., McNorton, J., Miller, P. A., Melton, J. R., Morino, I., Müller, J., Murguia-Flores, F., Naik, V., Niwa, Y., Noce, S., O'Doherty, S., Parker, R. J., Peng, C., Peng, S., Peters, G. P., Prigent, C., Prinn, R., Ramonet, M., Regnier, P., Riley, W. J., Rosentreter, J. A., Segers, A., Simpson, I. J., Shi, H., Smith, S. J., Steele, L. P., Thornton, B. F., Tian, H., Tohjima, Y., Tubiello, F. N., Tsuruta, A., Viovy, N., Voulgarakis, A., Weber, T. S., van Weele, M., van der Werf, G. R., Weiss, R. F., Worthy, D., Wunch, D., Yin, Y., Yoshida, Y., Zhang, W., Zhang, Z., Zhao, Y., Zheng, B., Zhu, Q., Zhu, Q., and Zhuang, Q.: The Global Methane Budget 2000–2017, Earth System Science Data, 12, 1561–1623, https://doi.org/10.5194/essd-12-1561-2020, 2020.

https://doi.org/10.5194/egusphere-2026-5476
Preprint. Discussion started: 11 September 2026

Saunois, M., Martinez, A., Poulter, B., Zhang, Z., Raymond, P. A., Regnier, P., Canadell, J. G., Jackson, R. B., Patra, P. K., Bousquet, P., Ciais, P., Dlugokencky, E. J., Lan, X., Allen, G. H., Bastviken, D., Beerling, D. J., Belikov, D. A., Blake, D. R., Castaldi, S., Crippa, M., Deemer, B. R., Dennison, F., Etiope, G., Gedney, N., Höglund-Isaksson, L., Holgerson, M. A., Hopcroft, P. O., Hugelius, G., Ito, A., Jain, A. K., Janardanan, R., Johnson, M. S., Kleinen, T., Krummel, P. B., Lauerwald, R., Li, T., Liu, X., McDonald, K. C., Melton, J. R., Mühle, J., Müller, J., Murguia-Flores, F., Niwa, Y., Noce, S., Pan, S., Parker, R. J., Peng, C., Ramonet, M., Riley, W. J., Rocher-Ros, G., Rosentreter, J. A., Sasakawa, M., Segers, A., Smith, S. J., Stanley, E. H., Thanwerdas, J., Tian, H., Tsuruta, A., Tubiello, F. N., Weber, T. S., van der Werf, G. R., Worthy, D. E. J., Xi, Y., Yoshida, Y., Zhang, W., Zheng, B., Zhu, Q., Zhu, Q., and Zhuang, Q.: Global Methane Budget 2000–2020, Earth System Science Data, 17, 1873–1958, https://doi.org/10.5194/essd-17-1873-2025, 2025.

Seinfeld, J. H. and Pandis, S. N.: Atmospheric chemistry and physics: from air pollution to climate change, John Wiley & Sons, ISBN ISBN: 978-1-118-94740-1, 2016.

Sharkey, T. D. and Singsaas, E. L.: Why plants emit isoprene, Nature, 374, 769, https://doi.org/10.1038/374769a0, 1995.

Sherwen, T., Schmidt, J. A., Evans, M. J., Carpenter, L. J., Großmann, K., Eastham, S. D., Jacob, D. J., Dix, B., Koenig, T. K., Sinreich, R., Ortega, I., Volkamer, R., Saiz-Lopez, A., Prados-Roman, C., Mahajan, A. S., and Ordóñez, C.: Global impacts of tropospheric halogens (Cl, Br, I) on oxidants and composition in GEOS-Chem, Atmospheric Chemistry and Physics, 16, 12 239–12 271, https://doi.org/10.5194/acp-16-12239-2016, 2016.

Singer, C. E. and Pincus, R.: Southern Ocean Clear-Sky Brightening From Sea Spray Aerosol Increase Drives Departure From Hemispheric Albedo Symmetry, Geophysical Research Letters, 53, e2025GL119 637, https://doi.org/10.1029/2025GL119637, 2026.

Skeie, R. B., Hodnebrog, Ø., and Myhre, G.: Trends in atmospheric methane concentrations since 1990 were driven and modified by anthropogenic emissions, Communications Earth & Environment, 4, 317, https://doi.org/10.1038/s43247-023-00969-1, 2023.

Song, S.-K., Shon, Z.-H., Choi, Y.-N., Son, Y.-B., Kang, M., Han, S.-B., and Bae, M.-S.: Global trend analysis in primary and secondary production of marine aerosol and aerosol optical depth during 2000–2015, Chemosphere, 224, 417–427, https://doi.org/10.1016/j.chemosphere.2019.02.152, 2019.

Soulie, A., Granier, C., Darras, S., Zilbermann, N., Doumbia, T., Guevara, M., Jalkanen, J.-P., Keita, S., Liousse, C., Crippa, M., Guizzardi, D., Hoesly, R., and Smith, S. J.: Global anthropogenic emissions (CAMS-GLOB-ANT) for the Copernicus Atmosphere Monitoring Service simulations of air quality forecasts and reanalyses, Earth System Science Data, 16, 2261–2279, https://doi.org/10.5194/essd-16-2261-2024, 2024.

Stevenson, D. S., Zhao, A., Naik, V., O'Connor, F. M., Tilmes, S., Zeng, G., Murray, L. T., Collins, W. J., Griffiths, P. T., Shim, S., Horowitz, L. W., Sentman, L. T., and Emmons, L.: Trends in global tropospheric hydroxyl radical and methane lifetime since 1850 from AerChemMIP, Atmospheric Chemistry and Physics, 20, 12 905–12 920, https://doi.org/10.5194/acp-20-12905-2020, 2020.

Strawson, I., Faïn, X., Bauska, T. K., Muschitiello, F., Vladimirova, D. O., Tetzner, D. R., Humby, J., Thomas, E. R., Liu, P., Zhang, B., Grilli, R., and Rhodes, R. H.: Historical Southern Hemisphere biomass burning variability inferred from ice core carbon monoxide records, Proceedings of the National Academy of Sciences, 121, e2402868 121, https://doi.org/10.1073/pnas.2402868121, 2024.

Swinnerton, J. W., Linnenbom, V. J., and Lamontagne, R. A.: The Ocean: A Natural Source of Carbon Monoxide, Science, 167, 984–986, https://doi.org/10.1126/science.167.3920.984, 1970.

The International GEOS-Chem User Community: geoschem/GCClassic: GCClassic 14.4.3, https://doi.org/10.5281/zenodo.13314490, 2024.

Thompson, A. M.: Wet and dry removal of tropospheric formaldehyde at a coastal site, Tellus, 32, 376–383, https://doi.org/10.1111/j.2153-3490.1980.tb00964.x, 1980.

https://doi.org/10.5194/egusphere-2026-5476
Preprint. Discussion started: 11 September 2026

Thompson, C. R., Wofsy, S. C., Prather, M. J., Newman, P. A., Hanisco, T. F., Ryerson, T. B., Fahey, D. W., Apel, E. C., Brock, C. A., Brune, W. H., Froyd, K., Katich, J. M., Nicely, J. M., Peischl, J., Ray, E., Veres, P. R., Wang, S., Allen, H. M., Asher, E., Bian, H., Blake, D., Bourgeois, I., Budney, J., Bui, T. P., Butler, A., Campuzano-Jost, P., Chang, C., Chin, M., Commane, R., Correa, G., Crounse, J. D., Daube, B., Dibb, J. E., DiGangi, J. P., Diskin, G. S., Dollner, M., Elkins, J. W., Fiore, A. M., Flynn, C. M., Guo, H., Hall, S. R., Hannun, R. A., Hills, A., Hintsa, E. J., Hodzic, A., Hornbrook, R. S., Huey, L. G., Jimenez, J. L., Keeling, R. F., Kim, M. J., Kupc, A., Lacey, F., Lait, L. R., Lamarque, J.-F., Liu, J., McKain, K., Meinardi, S., Miller, D. O., Montzka, S. A., Moore, F. L., Morgan, E. J., Murphy, D. M., Murray, L. T., Nault, B. A., Neuman, J. A., Nguyen, L., Gonzalez, Y., Rollins, A., Rosenlof, K., Sargent, M., Schill, G., Schwarz, J. P., Clair, J. M. S., Steenrod, S. D., Stephens, B. B., Strahan, S. E., Strode, S. A., Sweeney, C., Thames, A. B., Ullmann, K., Wagner, N., Weber, R., Weinzierl, B., Wennberg, P. O., Williamson, C. J., Wolfe, G. M., and Zeng, L.: The NASA Atmospheric Tomography (ATom) mission: Imaging the chemistry of the global atmosphere, Bulletin of the American Meteorological Society, 103, E761–E790, https://doi.org/10.1175/BAMS-D-20-0315.1, 2022.

Thoning, K. W., Tans, P. P., and Komhyr, W. D.: Atmospheric carbon dioxide at Mauna Loa Observatory: 2. Analysis of the NOAA GMCC data, 1974–1985, Journal of Geophysical Research: Atmospheres, 94, 8549–8565, https://doi.org/10.1029/JD094iD06p08549, 1989.

Tsivlidou, M., Sauvage, B., Bennouna, Y., Blot, R., Boulanger, D., Clark, H., Le Flochmoën, E., Nédélec, P., Thouret, V., Wolff, P., and Barret, B.: Tropical tropospheric ozone and carbon monoxide distributions: characteristics, origins, and control factors, as seen by IAGOS and IASI, Atmospheric Chemistry and Physics, 23, 14 039–14 063, https://doi.org/10.5194/acp-23-14039-2023, 2023.

Turner, A. J., Frankenberg, C., Wennberg, P. O., and Jacob, D. J.: Ambiguity in the causes for decadal trends in atmospheric methane and hydroxyl, Proceedings of the National Academy of Sciences, 114, 5367–5372, https://doi.org/10.1073/pnas.1616020114, 2017.

Turner, A. J., Frankenberg, C., and Kort, E. A.: Interpreting contemporary trends in atmospheric methane, Proceedings of the National Academy of Sciences, 116, 2805–2813, https://doi.org/10.1073/pnas.1814297116, 2019.

UCAR/NCAR - Earth Observing Laboratory: NSF/NCAR GV HIAPER Aircraft, https://doi.org/10.5065/D6DR2SJP, accessed: 2026-02-25, 2005.

UCAR/NCAR - Earth Observing Laboratory: HIPPO HIAPER Pole-to-Pole Observations, https://www.eol.ucar.edu/field_projects/hippo, accessed: 2026-02-25, 2011.

United Nations Department of Economic and Social Affairs, Population Division: World Population Prospects 2022: Summary of Results, Report UN DESA/POP/2022/TR/NO. 3, United Nations, New York, NY, https://social.desa.un.org/publications/world-population-prospects-2022-summary-of-results, 2022.

van der Velde, I. R., van der Werf, G. R., van Wees, D., Schutgens, N. A. J., Vernooij, R., Houweling, S., Tonucci, E., Chuvieco, E., Randerson, J. T., Frey, M. M., Borsdorff, T., and Aben, I.: Small Fires, Big Impact: Evaluating Fire Emission Estimates in Southern Africa Using New Satellite Imagery of Burned Area and Carbon Monoxide, Geophysical Research Letters, 51, e2023GL106 122, https://doi.org/10.1029/2023GL106122, 2024.

van der Werf, G. R., Randerson, J. T., Giglio, L., van Leeuwen, T. T., Chen, Y., Rogers, B. M., Mu, M., van Marle, M. J. E., Morton, D. C., Collatz, G. J., Yokelson, R. J., and Kasibhatla, P. S.: Global fire emissions estimates during 1997–2016, Earth System Science Data, 9, 697–720, https://doi.org/10.5194/essd-9-697-2017, 2017.

van der Zwaan, B., Kober, T., Longa, F. D., van der Laan, A., and Jan Kramer, G.: An integrated assessment of pathways for low-carbon development in Africa, Energy Policy, 117, 387–395, https://doi.org/10.1016/j.enpol.2018.03.017, 2018.

https://doi.org/10.5194/egusphere-2026-5476
Preprint. Discussion started: 11 September 2026

Vohra, K., Marais, E. A., Bloss, W. J., Schwartz, J., Mickley, L. J., Damme, M. V., Clarisse, L., and Coheur, P.-F.: Rapid rise in premature mortality due to anthropogenic air pollution in fast-growing tropical cities from 2005 to 2018, Science Advances, 8, eabm4435, https://doi.org/10.1126/sciadv.abm4435, 2022.

Škerlak, B., Sprenger, M., and Wernli, H.: A global climatology of stratosphere–troposphere exchange using the ERA-Interim data set from 1979 to 2011, Atmospheric Chemistry and Physics, 14, 913–937, https://doi.org/10.5194/acp-14-913-2014, 2014.

Wang, X., Jacob, D. J., Eastham, S. D., Sulprizio, M. P., Zhu, L., Chen, Q., Alexander, B., Sherwen, T., Evans, M. J., Lee, B. H., Haskins, J. D., Lopez-Hilfiker, F. D., Thornton, J. A., Huey, G. L., and Liao, H.: The role of chlorine in global tropospheric chemistry, Atmospheric Chemistry and Physics, 19, 3981–4003, https://doi.org/10.5194/acp-19-3981-2019, 2019.

Wang, X., Jacob, D. J., Downs, W., Zhai, S., Zhu, L., Shah, V., Holmes, C. D., Sherwen, T., Alexander, B., Evans, M. J., Eastham, S. D., Neuman, J. A., Veres, P. R., Koenig, T. K., Volkamer, R., Huey, L. G., Bannan, T. J., Percival, C. J., Lee, B. H., and Thornton, J. A.: Global tropospheric halogen (Cl, Br, I) chemistry and its impact on oxidants, Atmospheric Chemistry and Physics, 21, 13 973–13 996, https://doi.org/10.5194/acp-21-13973-2021, 2021.

Weinstock, B.: Carbon monoxide: Residence time in the atmosphere, Science, 166, 224–225, https://doi.org/10.1126/science.166.3902.224, 1969.

Wofsy, S., Afshar, S., Allen, H., Apel, E., Asher, E., Barletta, B., Bent, J., Bian, H., Biggs, B., Blake, D., Blake, N., Bourgeois, I., Brock, C., Brune, W., Budney, J., Bui, T., Butler, A., Campuzano-Jost, P., Chang, C., Chin, M., Commane, R., Correa, G., Crounse, J., Cullis, P. D., Daube, B., Day, D., Dean-Day, J., Dibb, J., DiGangi, J., Diskin, G., Dollner, M., Elkins, J., Erdesz, F., Fiore, A., Flynn, C., Froyd, K., Gesler, D., Hall, S., Hanisco, T., Hannun, R., Hills, A., Hintsa, E., Hoffman, A., Hornbrook, R., Huey, L., Hughes, S., Jimenez, J., Johnson, B., Katich, J., Keeling, R., Kim, M., Kupc, A., Lait, L., McKain, K., Mclaughlin, R., Meinardi, S., Miller, D., Montzka, S., Moore, F., Morgan, E., Murphy, D., Murray, L., Nault, B., Neuman, J., Newman, P., Nicely, J., Pan, X., Paplawsky, W., Peischl, J., Prather, M., Price, D., Ray, E., Reeves, J., Richardson, M., Rollins, A., Rosenlof, K., Ryerson, T., Scheuer, E., Schill, G., Schroder, J., Schwarz, J., St.Clair, J., Steenrod, S., Stephens, B., Strode, S., Sweeney, C., Tanner, D., Teng, A., Thames, A., Thompson, C., Ullmann, K., Veres, P., Wagner, N., Watt, A., Weber, R., Weinzierl, B., Wennberg, P., Williamson, C., Wilson, J., Wolfe, G., Woods, C., Zeng, L., and Vieznor, N.: ATom: Merged Atmospheric Chemistry, Trace Gases, and Aerosols, Version 2, https://doi.org/10.3334/ORNLDAAC/1925, [Dataset], 2021.

Wofsy, S. C., HIPPO Science Team, and Cooperating Modellers and Satellite Teams: HIAPER Pole-to-Pole Observations (HIPPO): fine-grained, global-scale measurements of climatically important atmospheric gases and aerosols, Philosophical Transactions of the Royal Society A: Mathematical, Physical and Engineering Sciences, 369, 2073–2086, https://doi.org/10.1098/rsta.2010.0313, 2011.

Wofsy, S. C., Daube, B. C., Jimenez, R., Kort, E., Pittman, J. V., Park, S., Commane, R., Xiang, B., Santoni, G., Jacob, D., Fisher, J., Pickett-Heaps, C., Wang, H., Wecht, K., Wang, Q.-Q., Stephens, B. B., Shertz, S., Watt, A. S., Romashkin, P., Campos, T., Haggerty, J., Cooper, W. A., Rogers, D., Beaton, S., Hendershot, R., Elkins, J. W., Fahey, D. W., Gao, R. S., Moore, F., Montzka, S. A., Schwarz, J. P., Perring, A. E., Hurst, D., Miller, B. R., Sweeney, C., Oltmans, S., Nance, D., Hintsa, E., Dutton, G., Watts, L. A., Spackman, J. R., Rosenlof, K. H., Ray, E. A., Hall, B., Zondlo, M. A., Diao, M., Keeling, R., Bent, J., Atlas, E. L., Lueb, R., and Mahoney, M. J.: HIPPO Merged 10-second Meteorology, Atmospheric Chemistry, and Aerosol Data, Version 1.0, https://doi.org/10.3334/CDIAC/HIPPO_010, [Dataset], 2017.

Worden, H. M., Deeter, M. N., Edwards, D. P., Gille, J. C., Drummond, J. R., and Nédélec, P.: Observations of near-surface carbon monoxide from space using MOPITT multispectral retrievals, Journal of Geophysical Research: Atmospheres, 115, https://doi.org/10.1029/2010JD014242, 2010.

Worden, H. M., Deeter, M. N., Frankenberg, C., George, M., Nichitiu, F., Worden, J., Aben, I., Bowman, K. W., Clerbaux, C., Coheur, P. F., de Laat, A. T. J., Detweiler, R., Drummond, J. R., Edwards, D. P., Gille, J. C., Hurtmans, D., Luo, M., Martínez-Alonso, S., Massie,

https://doi.org/10.5194/egusphere-2026-5476
Preprint. Discussion started: 11 September 2026

S., Pfister, G., and Warner, J. X.: Decadal record of satellite carbon monoxide observations, Atmospheric Chemistry and Physics, 13, 837–850, https://doi.org/10.5194/acp-13-837-2013, 2013.

World Data Center for Greenhouse Gases (WDCGG): CO, https://gaw.kishou.go.jp/search, accessed: 2026-07-15, 2025.

World Meteorological Organization: WMO WDCGG Data Summary, WDCGG No. 49: Greenhouse and Related Gases, Tech. rep., published in co-operation with the World Meteorological Organization Global Atmosphere Watch, World Data Centre for Greenhouse Gases, 2025.

Yan, J., Jung, J., Lin, Q., Zhang, M., Xu, S., and Zhao, S.: Effect of sea ice retreat on marine aerosol emissions in the Southern Ocean, Antarctica, Science of The Total Environment, 745, 140 773, https://doi.org/10.1016/j.scitotenv.2020.140773, 2020.

Yang, L. H., Jacob, D. J., Lin, H., Dang, R., Bates, K. H., East, J. D., Travis, K. R., Pendergrass, D. C., and Murray, L. T.: Assessment of Hydrogen's Climate Impact Is Affected by Model OH Biases, Geophysical Research Letters, 52, e2024GL112 445, https://doi.org/https://doi.org/10.1029/2024GL112445, 2025.

Yin, Y., Chevallier, F., Ciais, P., Broquet, G., Fortems-Cheiney, A., Pison, I., and Saunois, M.: Decadal trends in global CO emissions as seen by MOPITT, Atmospheric Chemistry and Physics, 15, 13 433–13 451, https://doi.org/10.5194/acp-15-13433-2015, 2015.

Yoon, J. and Pozzer, A.: Model-simulated trend of surface carbon monoxide for the 2001–2010 decade, Atmospheric Chemistry and Physics, 14, 10 465–10 482, https://doi.org/10.5194/acp-14-10465-2014, 2014.

Yoon, J. Y. S., Wells, K. C., Millet, D. B., Swann, A. L. S., Thornton, J., and Turner, A. J.: Impacts of Interannual Isoprene Variations on Methane Lifetimes and Trends, Geophysical Research Letters, 52, e2025GL114 712, https://doi.org/10.1029/2025GL114712, 2025.

Yvon-Durocher, G., Allen, A. P., Bastviken, D., Conrad, R., Gudasz, C., St-Pierre, A., Thanh-Duc, N., and del Giorgio, P. A.: Methane fluxes show consistent temperature dependence across microbial to ecosystem scales, Nature, 507, 488–491, https://doi.org/10.1038/nature13164, 2014.

Zhao, Y., Saunois, M., Bousquet, P., Lin, X., Hegglin, M. I., Canadell, J. G., Jackson, R. B., and Zheng, B.: Reconciling the bottom-up and top-down estimates of the methane chemical sink using multiple observations, Atmospheric Chemistry and Physics, 23, 789–807, https://doi.org/10.5194/acp-23-789-2023, 2023.

Zheng, B., Chevallier, F., Yin, Y., Ciais, P., Fortems-Cheiney, A., Deeter, M. N., Parker, R. J., Wang, Y., Worden, H. M., and Zhao, Y.: Global atmospheric carbon monoxide budget 2000–2017 inferred from multi-species atmospheric inversions, Earth System Science Data, 11, 1411–1436, https://doi.org/10.5194/essd-11-1411-2019, 2019.

Zheng, B., Ciais, P., Chevallier, F., Chuvieco, E., Chen, Y., and Yang, H.: Increasing forest fire emissions despite the decline in global burned area, Science advances, 7, eabh2646, https://doi.org/10.1126/sciadv.abh2646, 2021.

Zheng, C., Li, X., Azorin-Molina, C., Li, C., Wang, Q., Xiao, Z., Yang, S., Chen, X., and Zhan, C.: Global trends in oceanic wind speed, wind-sea, swell, and mixed wave heights, Applied Energy, 321, 119 327, https://doi.org/10.1016/j.apenergy.2022.119327, 2022.